

# A Review on Quantum Dot-Based Color Conversion Layers for Mini/Micro-LED Displays: Packaging, Light Management, and Pixelation

Junchi Chen, Qiliang Zhao, Binhai Yu,\* and Uli Lemmer\*

Mini/microlight-emitting diodes (LEDs) are one of the most promising technologies for next-generation displays to meet the requirements of demanding applications, including augmented reality/virtual reality displays, wearable devices, and microprojectors. To realize full-color displays, the strategy of combining miniaturized blue nitride-based LEDs with color conversion layers is promising due to the high efficiencies of the LEDs and the advantageous manufacturing. Quantum dots (QDs), owing to their high photoluminescence quantum yield, small particle size, and solution processability, have emerged as the color conversion material with the most potential for mini/micro-LEDs. However, the integration of QDs into display technologies poses several challenges. From the material side, the stability of QD materials is still challenging. For the case of packaging QDs in a matrix, the dispersion quality of QDs and the light extraction of the emission need to be improved. From the fabrication side, the lack of high-precision mass manufacturing strategies in QD pixelation hinders the widespread application of QDs. Toward the issues above, this review summarizes the research on QD materials for color conversion display in recent years to systematically draw an overview of the packaging strategies, the light management approaches, and the pixelation methods of QD materials toward mini/micro-LED-based display technologies.

## 1. Introduction

Mini/microlight-emitting diodes (LEDs), i.e., miniaturized gallium nitride (GaN)-based LEDs, have been widely developed for high-performance displays in recent years. The LEDs with sizes ranging from 100 to 200  $\mu\text{m}$  are usually called mini-LEDs, and those with dimensions less than 100  $\mu\text{m}$  are called micro-LEDs.<sup>[1]</sup> The targeted applications of mini-LEDs are large-scale outdoor displays or backlight modules for liquid crystal displays (LCDs) to optimize their performance.<sup>[2]</sup> Micro-LEDs, on the other hand, will have widespread applications for active indoor displays or small-sized screens for intelligent devices. Micro-LED technology made rapid advances in the last two decades. It became a field of intense research after the initial fabrication of a 12  $\mu\text{m}$   $\times$  12  $\mu\text{m}$  micro-LED chip in 2000.<sup>[3]</sup> Despite the remaining challenges for mass fabrication and packaging, Mini/micro-LEDs have obvious advantages compared to LCD, organic LED (OLED), and other display technologies owing to their high brightness, high contrast ratio, and high display resolution.<sup>[4–6]</sup>

Mini/micro-LED technologies can be applied in a variety of fields, including cell phones, wearable smart devices, high-end TVs, visible light communication, augmented reality (AR) or virtual reality (VR) devices, and head-mounted displays.<sup>[7,8]</sup> Moreover, owing to their small size, micro-LEDs can be used in flexible displays by adapting to a flexible substrate. According to a report published by Research and Markets (a market research firm), the micro-LED market is expected to grow at a compound annual growth rate of 89.3%, from \$409 million in 2020 to \$18.835 billion by 2026.<sup>[9]</sup> In the global arena, companies including Sony, Samsung, Apple, and BOE have invested heavily in research on micro-LED technology. However, mini/micro-LED display technologies still face many obstacles. Four key technologies are the most critical ones: miniaturization technology, giant transfer technology, junction bonding technology, and red–green–blue (RGB) colorization technology.<sup>[10–12]</sup> Regarding RGB colorization technology, it is not efficient for mini/micro-LEDs to directly utilize LED chips that emit three primary colors for full-color display. Phosphide-based LEDs are prone to defects in the epitaxial preparation of light-emitting layer materials for higher bandgaps,

J. Chen, U. Lemmer  
Light Technology Institute  
Karlsruhe Institute of Technology (KIT)  
Engesserstrasse, 13, 76131 Karlsruhe, Germany  
E-mail: uli.lemmer@kit.edu

Q. Zhao, B. Yu  
National and Local Joint Engineering Research Center of Semiconductor Display and Optical Communication Devices  
South China University of Technology (SCUT)  
Guangzhou 510640, China  
E-mail: mebhaiyu@scut.edu.cn

 The ORCID identification number(s) for the author(s) of this article can be found under <https://doi.org/10.1002/adom.202300873>

© 2023 The Authors. Advanced Optical Materials published by Wiley-VCH GmbH. This is an open access article under the terms of the Creative Commons Attribution-NonCommercial License, which permits use, distribution and reproduction in any medium, provided the original work is properly cited and is not used for commercial purposes.

DOI: 10.1002/adom.202300873

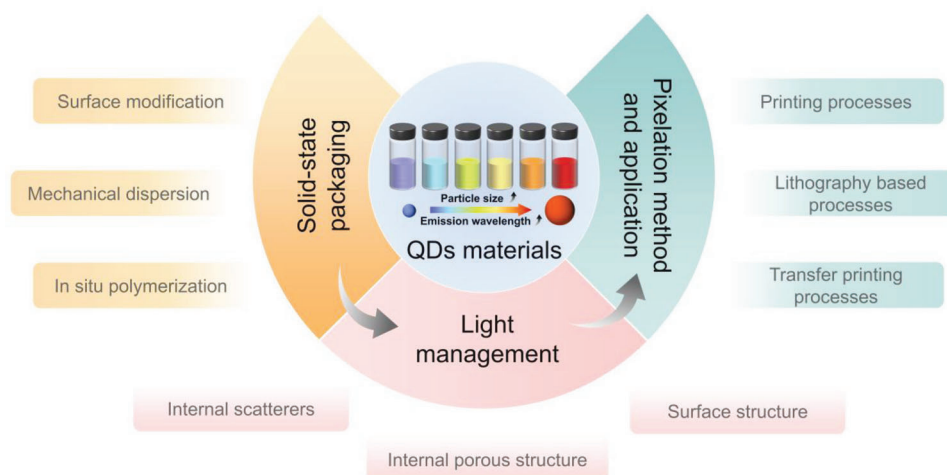


**Figure 1.** Illustration of the structure of this review: relevant to the theme of patterned QD films, recent research is introduced on the topics of QD materials, solid-state packaging of QDs, light management of QD films, and preparation of pixelated QDs.

which result in high manufacturing difficulty and reduced lifetimes. AlGaInP, as the most used red-emitting LED material, suffers from a serious efficiency decrease caused by sidewall effect when being miniaturized as required for mini-/micro-LEDs.<sup>[13,14]</sup> At the same time, green GaN LEDs suffer from low external quantum efficiency (EQE), called the “green gap.”<sup>[5,15,16]</sup> By contrast, blue GaN LEDs are more viable due to the advantages of having high luminous efficiency, high manufacturing maturity, and low costs. RGB colorization can be efficiently achieved based on blue mini-/micro-LED by coating a photoluminescent medium, which acts as a color converter.<sup>[17]</sup> In addition, this strategy reduces the technical requirement for giant transfer technology as the transfer and alignment process has only to be solved for one type of chips (blue chips) rather than for three types (RGB chips).

For colorization, rare-earth phosphors are widely used to encapsulate conventional LEDs at the present stage.<sup>[18–20]</sup> However, the relatively large particle size of typical phosphors (generally 1–10 μm) inhibits their uniform coating on the micro-LEDs.<sup>[21]</sup> As an emerging color conversion material, quantum dots (QDs) seem to better meet the needs of mini-/micro-LED-based full-color display technologies due to their small particle size, high photoluminescence quantum yield (PLQY), narrow emission half-peak width, and solution processability.<sup>[22–26]</sup> Many studies have been reported on QD materials in various fields, including displays, lasers, solar cells, and biomedical photonics.<sup>[27–30]</sup> However, several problems remain unsolved when applying QD materials in high-performance mini-/micro-LED display devices. First, from the material side, optical performance measures such as the PLQY and luminescence stability need to be further improved. Second, to ensure adequate stability as well as to obtain better processability, QDs are usually packaged in a solid-state medium. During the packaging, the agglomeration-induced luminescence quenching and the mismatching between ligands and matrix limit the efficiency of QDs.<sup>[31–33]</sup> Third, to meet the demand for high-resolution display technology, an efficient and high-precision fabrication method for RGB QD pixel arrays needs to be further developed for industrialization. Finally, appropriate light management for improving light extraction also needs to be developed.

Toward the new requirements for mini-/micro-LED display technologies, this review summarizes the research on QD materials and display applications in recent years from three perspectives: packaging, light management, and pixelation method. As shown in **Figure 1**, we first summarize the properties of QD materials commonly used in the display field. Then, regarding the solid-state packaging of QD materials, we mainly focus on research to enhance the dispersibility and stability of QDs in a solid-state matrix. Furthermore, we summarize recent research on light management for photoluminescence (PL) enhancement of QD color conversion layers using nano/microstructures. Finally, this review summarizes recent research on QD pixelation approaches and their applications in mini-/micro-LED display technology.

## 2. Properties of QDs

In 1981, Ekimov and Onushchenko demonstrated the quantum size effect on CuCl nanocrystals grown in a transparent dielectric matrix.<sup>[34]</sup> In the same year, Grätzel and co-workers successfully synthesized colloidal CdS in an aqueous solution.<sup>[35]</sup> Subsequently, Brus and co-workers demonstrated that the Raman resonance and absorption spectra of colloidal CdS nanoparticles could be altered by changing the particle size, thereby lifting the curtain of QD materials.<sup>[36]</sup> Since the 1980s, QD materials have attracted increasing attention.<sup>[37–39]</sup> In 1994, Alivisatos and co-workers reported a CdSe QD LED combined with a semiconducting polyphenylene vinylene polymer.<sup>[40]</sup> It promoted the application of QD materials in the LED and display areas.

Nowadays, besides luminescence performance, the stability of QDs is another vital parameter hindering their development. Valuable efforts from the following researchers have been made for promoting the efficiency of QDs while maintaining decent stability. Packaging QDs in one or more shell structures to obtain core-shell nanoparticles, such as CdSe/ZnS QDs and CdSe/CdS/ZnS/CdSZnS QDs, has been market-tested as a straightforward and effective strategy. By changing the materials and parameters of the shell structure, the electron states and

**Table 1.** Properties of several common types of QDs.

	Peak emission [nm]	FWHM [nm]	PLQY [%]	Refs.
CdSe	Tunable	28–32	$\approx 99.6 \pm 0.2$	[43]
CdSe	532 (green)	26	75	[44]
ZnCdSe	630 (red)	17.1	99	[45]
CdZnS	455 (blue)	17.2	92	[46]
InP	$\approx 535$ (green)	37	95	[47]
InP	630 (red)	35	$\approx 100$	[48]
(InP/ZnSe/ZnS)				
InP	$\approx 425$ (blue)	$\approx 72$	$\approx 25$	[49]
(InP/ZnS)				
Perovskite (MAPbBr <sub>3</sub> )	526 (green)	20	$\approx 100$	[52]
Perovskite (CsPbBr <sub>x</sub> Cl <sub>3-x</sub> )	463 (blue)	15	98	[54]
Perovskite (CsPbI <sub>3</sub> )	680 (red)	33	96	[55]

optical performances of QDs can also be tuned.<sup>[41]</sup> In 1996, Hines and Guyot-Sionnest proposed a synthesis of ZnS-capped CdSe QDs using organometallic reagents. A PLQY value of 50% was achieved at room temperature, which was an order of magnitude higher than that of CdSe QDs without capping.<sup>[42]</sup> Moreover, the presence of a shell structure enhances the adaptivity of QDs with different ligands, which can improve the surface chemical properties and processability of QDs.

## 2.1. Luminescence Performance

Among the various types of QDs, CdSe/S-based, and InP-based, are the most commonly used for lighting and displays. More recently, perovskite QDs have also been intensely studied in different research laboratories. Here, we summarize some highlight performances of these three groups of QD materials reported in recent years (Table 1). It can be seen that QD materials generally have a narrow FWHM and high PLQY. Cd-based QDs have been developed over two decades and are more mature than other types of QDs. These QDs have the potential to better meet the requirements of commercial applications because of their high stability and excellent PLQY of up to almost 100% in solution. Hanif et al. developed a photothermal threshold quantum yield measurement method to obtain extremely accurate PLQY data with an optimal uncertainty of 0.04%. Using this method, the PLQY of a synthesized CdSe/CdS core-shell QD was measured to be  $99.6\% \pm 0.2\%$ . The particle comprised nominally 8.5 monolayers of shell capping and almost no nonradiative decay was observed.<sup>[43]</sup> The thick-shell QDs (TSQDs) prepared by Delville and co-workers exhibited a narrow FWHM of  $\approx 26$  nm, with an emission peak wavelength of 532 nm. The TSQDs were prepared by introducing tri-*N*-octylphosphine as the ligand and solvent during the synthesis of CdSe QDs to remove excess Cd<sup>2+</sup> ions on the surface of the CdSe cores and repair surface lattice defects, followed by a multilayer ZnS shell-coating process.<sup>[44]</sup> In addition, various Cd-based QD materials have been derived based on CdSe QDs. Jin et al. proposed a cation exchange-assisted exfoliation

method to convert the CdSe core into a ZnCdSe alloy core and obtained ZnCdSe/ZnSe core-shell QDs. The ZnCdSe/ZnSe, core-shell QDs, exhibited excellent optical performance with a small FWHM (17.1 nm) and high PLQY (99%).<sup>[45]</sup> Li and co-workers successfully synthesized blue-emitting CdZnS/ZnS QDs with both a high PLQY (up to 92%) and narrow FWHM (<18 nm) using an efficient one-pot method.<sup>[46]</sup>

Nevertheless, the high toxicity of the Cd-based QDs is problematic for commercial applications.<sup>[22]</sup> Thus, considerable effort has been devoted to develop cadmium-free QDs as replacements. InP-based QDs are the most promising candidates. However, owing to their relatively short development time and the complexity of the synthesis, the overall optical performance of In-based QDs is poorer than that of Cd-based QDs, especially for blue-emitting QDs. In a recent study, high-quality InP QDs (green: PLQY = 95%, FWHM = 37 nm; red: PLQY = 95%, FWHM = 37 nm) were synthesized by Park and co-workers by introducing a simple thermal treatment to the process to adjust the reactivity of the zinc carboxylate. As precursors, the zinc oxo clusters obtained from the thermal treatment could suppress the depletion of the highly reactive phosphorus to improve the size uniformity of the In(Zn)P core and facilitate the generation of an oxidized buffer layer effectively avoiding the formation of defects.<sup>[47]</sup> By suppressing the oxidative defects during the synthesis of QDs, Jang and co-workers successfully prepared red-emitting InP/ZnSe/ZnS (core/shell/shell) QDs with a PLQY  $\approx 100\%$  and an FWHM of 35 nm. To prevent oxidation during the synthesis, precursors and solvent were thoroughly purified by a vacuum heating treatment before the reaction. In addition, a protecting N<sub>2</sub> flow was applied during the reaction. Hydrofluoric acid was introduced to the solution for removing oxides during the growth of the shell structure.<sup>[48]</sup> The relatively poor controllability of the nucleation and growth during synthesis are a challenge for the development of blue-emitting InP QDs. Tian and co-workers proposed a synthesis approach with employing copper cations for confining the particle size of QDs, obtaining InP/ZnS core/shell QDs with an emitting peak at deep blue wavelength ( $\approx 425$  nm) and a PLQY  $\approx 25\%$ . With the presence of copper cations, Cu<sub>3-x</sub>P nanocrystals were produced as well during the nucleation of InP QDs that competitively inhibits the growth. Thus, particularly small InP QDs with deep blue emission were achieved.<sup>[49]</sup>

Perovskite QDs (PeQDs) are a group of QD materials with perovskite crystal structures. This class of materials benefits from the tremendous progress in the field of metal halogenide perovskite solar cells.<sup>[50,51]</sup> Compared to other QDs, PeQDs inherit the characteristics of bulk perovskite materials with tuneable bandgaps, simple low-temperature synthesis processes, and low manufacturing costs. In addition, the FWHM of PeQDs is generally less than 20 nm, and the PLQY can also be close to 100%. This enables high color purity and conversion efficiency. Compared to Cd-based QDs, PeQDs can achieve similar or even better optical performance. Therefore, PeQDs have attracted extensive attention in recent years. Lin and co-workers proposed a spray pyrolysis method for synthesizing high-performance organic-inorganic hybrid PeQDs, which exhibited a PLQY close to 100% and an FWHM of 20 nm. In their method, precursors of PeQDs with organic ligands (oleic acid and *n*-octylamine) were dissolved in dimethylformamide (DMF) and then sprayed into a poor

solvent (toluene). As the atomized microdroplets increased the contact with the poor solvent, a high crystal quality was achieved, and PeQDs with a homogeneous size were generated.<sup>[52]</sup> However, the stability of PeQDs exposed to water, oxygen, and heat is worse than the one of Cd- and In-based QDs. This is currently the biggest challenge for widespread applications. Moreover, PeQD materials are susceptible to crystal defects, which require careful synthesis and proper passivation. This effect is more evident for blue PeQDs, as they require a smaller particle size and, therefore, a larger specific surface area, leading to the appearance of a large number of surface defects and resulting in a much lower PLQY. For instance, the PLQY of blue-emitting CsPbBr<sub>x</sub>Cl<sub>3-x</sub> QDs is typically less than 50%.<sup>[53]</sup> To improve the efficiency of blue PeQDs, Yang and co-workers designed an ultrafast thermodynamic control strategy using liquid nitrogen that could instantaneously freeze the ideal crystal lattices of the PeQDs. This treatment led to the abrupt termination of further crystal growth and could also avoid additional nucleation at low temperatures, resulting in blue PeQDs with a PLQY of up to 98%.<sup>[54]</sup> However, this method is relatively complicated and increases fabrication costs. For red PeQDs, Cai et al. reported a synthesis method for bright and stable red emitting CsPbI<sub>3</sub> PeQDs with trimethylsilyl iodine through a reaction scheme with an I/Pb molar ratio of  $\approx 4.2$ . This method significantly improved the stability, maintaining the PLQY above 85%, with a maximum of greater than 96%, over 105 days.<sup>[55]</sup> Perovskite LEDs (PeLEDs) have attracted considerable research attention because of their excellent performance and great potential.<sup>[56]</sup>

To achieve high-performance display based on mini/micro-LEDs, different types of QDs are usually combined for coloration according to their luminescence performances and features. For instance, despite the limited lifetime, green-emitting PeQDs are commonly combined with red-emitting Cd-based QDs for wide-gamut full-color display in academic research, owing to their excellent PLQY and narrow FWHM on the corresponding emission wavelength.<sup>[57-59]</sup> Regarding the synthesis and preparation of QD materials, the current research focuses on reducing nonradiative recombination, such as Auger recombination and trap-assisted recombination, to improve luminescence performance.<sup>[60-62]</sup>

## 2.2. Stability of PeQDs

In addition to enhancing the optical performance, the stability of QDs against water, oxygen, and heat are critical to promote QD materials for commercial display applications. At the present stage, due to the higher formation energy and longer development time, Cd-based and InP-based QDs exhibit better stability than PeQDs. Some Cd-based and InP-based QDs with mature core-shell design have been successfully introduced to the market for several years.<sup>[63,64]</sup> By contrast, owing to the inherent ionic nature and low formation enthalpy, PeQDs are highly sensitive to environmental factors including moisture, oxygen, and heat, resulting in a poor stability and lifetime. Therefore, we limit our review on the stability of PeQDs here.

To improve the stability of the lattice of PeQDs, Kim et al. employed ion doping of nickel metal into synthesis process. The divalent nickel ions prefer octahedral coordination with halide ions and increase the formation enthalpy of PeQDs. With the

dose optimization of the nickel dopant, green-emitting PeQDs with a PLQY up to 82.9% were obtained. Moreover, the nickel-doped PeQDs show a lower PL reduction of 18% after 48 h of UV radiation (350  $\mu\text{W cm}^{-2}$ ), while the undoped PeQDs obtained a PL loss of 69.3%.<sup>[65]</sup> Ligand engineering is another efficient strategy for enhancing stability. Yang and co-workers proposed a multi-amine chelating ligand (*N'*-(2-aminoethyl)-*N'*-hexadecylethane-1,2-diamine, AHDA) with much higher binding energy (2.36 eV) than oleylammonium ligand (1.47 eV) when anchoring on the surface of CsPbI<sub>3</sub> PeQDs. Owing to the tough binding of the ligands, PeQD dispersion capped with AHDA retained most of the ligands after 15 repeated purification cycles. Moreover, the AHDA-capped PeQD film maintained its original perovskite  $\gamma$ -phase for over 20 days under the condition of annealing at 85 °C in air with a relative humidity of 30–40%. As a reference, the PeQD film capped with oleylammonium ligands transformed from perovskite  $\gamma$ -phase to non-perovskite  $\delta$ -phase within 2 days.<sup>[66]</sup> Organosilicon ligands can act as both the capping agent and the precursor for a silica matrix in the PeQD system. Sun et al. introduced (3-aminopropyl)triethoxysilane (APTES) ligands. In this method, the synthesis process of PeQDs was conducted in water-free environment, and when the system was opened to the air, the trace water vapor triggered the hydrolysis of APTES ligands for forming the silica matrix. With the silica coating, the PeQD films demonstrated a low decrease of the PLQY from 85% to 78% for green-emitting QDs and from 88% to 68% for red-emitting QDs, after a storage time of 90 days.<sup>[67]</sup> Besides silica-based matrixes, Li et al. proposed a straightforward encapsulation approach by employing anodic aluminum membrane (AAM) as the template for the deposition of PeQDs. By combining inkjet printing and vacuum deposition, PeQDs were filled into the nanohole array of AAM template. Benefitting from the high thermal conductivity of the AAM host, the PeQD/AAM composite film obtained excellent thermal stability. After the radiation of a high-power blue laser (power density of 108.54  $\text{mW mm}^{-1}$ ) for 80 s, the QD/AAM film exhibited a maximal temperature of 59.3 °C, while the maximal temperature of the bare PeQD film reached 91.6 °C.<sup>[68]</sup> Besides, solutions that combine multiple strategies above for improving the stability of PeQDs, such as the combination of ion doping and matrix encapsulation, were commonly proposed as well.

## 3. Solid-State Packaging of QDs

As a color conversion medium for mini/micro-LED display applications, QD materials are typically required to be attached to chips or made into a stable layer of an RGB pixel array. Because of the poor resistance of QD materials to water and oxygen, it is necessary to package QDs in a solid-state matrix composed of materials such as polymers, ionic crystals, or inorganic particles as protection. Because of their low thermal reliability, proper thermal packaging is vital for commercial QD applications.<sup>[69-72]</sup> However, the surface ligands of QDs usually show poor compatibility with the solid-state matrix, and directly mixing or embedding QD materials into the matrix is prone to uneven dispersion and aggregation because of the detachment of surface ligands, leading to luminescence quenching and degradation of the optical properties. It has been revealed that the reduction of the amino ligands attaching on the surface of CdSe QDs resulted in

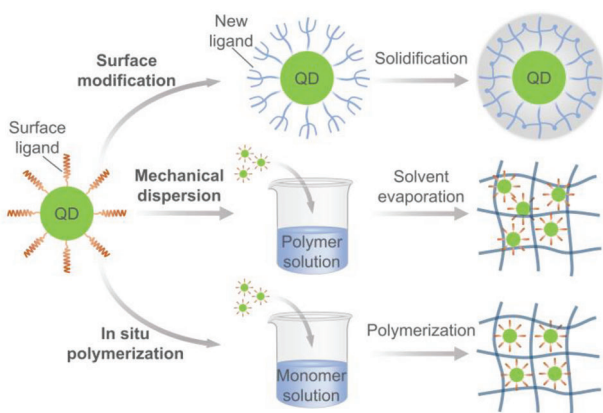


**Figure 2.** Scheme of the strategies for solid-state packaging of QDs.

a significant PLQY drop from 70% to 18%.<sup>[73]</sup> Moreover, Klimov and co-workers conducted a comprehensive study to investigate the influence of the capping ligands on the luminescence performance of the polymer-packaged QDs. In this study, six types of ligands (oleic acid, thioglycolic acid, 1,2-ethanediamine, hexamethylenediamine, amino-terminated polyether 400, and amino-terminated polyether 2000) were applied as the capping ligands for CdSe QDs, which were then mixed into epoxy as encapsulating matrix. Due to the different affinity of the six ligands for the epoxy matrix, different degrees of QD aggregation were observed and the resulting relative PL intensity of the films vary largely from 0.09 to 1.93.<sup>[74]</sup> The properties of the selected matrix material, such as thermal conductivity and water resistance, are crucial as well to the stability and lifetime of the QD color conversion layer. Therefore, the homogeneous encapsulation of QDs in an appropriate solid-state matrix is a foundation for QD-enhanced mini/micro-LED displays.

The existing strategies for solid-state packaging of QDs can be divided into three categories: surface modification, mechanical dispersion, and in situ polymerization. As shown in **Figure 2**, the schematics of the three packaging strategies are illustrated. Surface modification methods focus on the ligand engineering for improving the affinity between QDs and the outer matrix or employing cross-linkable ligands to directly form the coating shell. Mechanical dispersion methods directly mix the QD dispersion into a polymer solution by a mechanical process, such as magnetic stirring, or sonication. In situ polymerization methods first blend QD dispersion with the monomer solution, followed by a polymerization process of the monomer to solidify the polymer matrix.

### 3.1. Surface Modification

Ligands inherently cap the surfaces of QDs during and after synthesis. This protects the QDs and provides the possibility of bonding with other materials. Therefore, appropriate surface modification of QDs, such as forming a coating shell or introducing certain functional groups, can generate better bonding with the packaging medium. Dong and co-workers reported a QD/polymer composite ink with good dispersibility in water for inkjet printing. As shown in **Figure 3a,b**, they

utilized a dual functional group polymer, mercaptopropionic polyethyleneimine (MPPEI), with a thiol of 3-mercaptopropionic acid (MPA) and an amine of polyethyleneimine (PEI) to modify the surface of CdSe/CdS/ZnS core/shell/shell QDs. MPPEI reduced the oxidation of the thiol and improved the binding affinity of the amino group, thus providing adequate protection for the QDs. The obtained QD material exhibited excellent acid resistance, base resistance, photostability, and thermostability, enabling its application in anti-counterfeiting and identification.<sup>[75]</sup>

Wang and co-workers proposed a packaging method that combined the sol-gel method and the fluidized powder atomic layer deposition (ALD) technique to prepare ultrastable QD/SiO<sub>2</sub>/Al<sub>2</sub>O<sub>3</sub> luminescent microspheres (QLuMiS). Schematics of the method are shown in **Figure 3c,d**. They first obtained QD/SiO<sub>2</sub> particles through the hydrolysis of methoxysilane precursors in a CdZnSeS gradient alloy QD dispersion. An Al<sub>2</sub>O<sub>3</sub> coating layer was then grown on the surface of the QDs/SiO<sub>2</sub> particles via the ALD technique to obtain QLuMiS. The prepared QLuMiS maintained more than 86% of its PLQY after aging for 1000 h under blue light irradiation at 450 nm with an optical power density of 2000 mW cm<sup>-2</sup>, showing excellent stability. Moreover, in the same aging experiment, the extrapolated lifetime (LT50) of the QLuMiS was 4969 h, the best lifetime until 2022. By integrating the QLuMiS into a cell phone LCD module as a color conversion material, a wide NTSC color gamut of 115% was achieved. The excellent stability was attributed to the hydroxyl groups on the surface of the SiO<sub>2</sub> coating, which provided many chemisorption sites and facilitated the formation of a dense Al<sub>2</sub>O<sub>3</sub> layer in the ALD process; the Al<sub>2</sub>O<sub>3</sub> material is an excellent moisture and oxygen barrier that protects QDs from damage.<sup>[76]</sup>

QD materials can also be compounded with aerogel materials to achieve better dispersion and stability. Wang et al. chemically modified the surface of ZnS(CuInS<sub>2</sub>)/ZnS core-shell QDs using a new ligand, 3-(mercaptopropyl)trimethoxysilane (3-MPTMS), to generate stable covalent bonding between the QDs and bacterial cellulose (BC) after transferring the QDs from toluene to an alcohol solvent. After supercritical CO<sub>2</sub> drying, a QD/carbon nanotube aerogel was obtained. A schematic of this route is shown in **Figure 3e**. While maintaining the porous nanofiber morphology of ultralight carbon nanotubes, QDs were uniformly distributed along the surface of the carbon nanotube fibers without aggregation and achieved a PLQY of 35%.<sup>[77]</sup> BC with its nanofiber network structure is a suitable matrix for dispersing QD materials to overcome the fluorescence quenching effect of QD/polymer composites. The obtained quantum yield value with BC matrix is higher than the aerogel-encapsulated ZnS(CuInS<sub>2</sub>)/ZnS QDs, which exhibited a maximal PLQY of 30%.<sup>[78]</sup>

### 3.2. Mechanical Dispersion

Mechanical dispersion is the most straightforward method for embedding QDs into a functional film. The principle is to utilize organic solvents that disperse the QDs well and solve the packaging matrix to act as intermediates for the luminescent medium and the protective matrix. Following a stirring process for homogeneous mixing and sufficient evaporation of the organic solvent, QDs can be embedded into the remaining

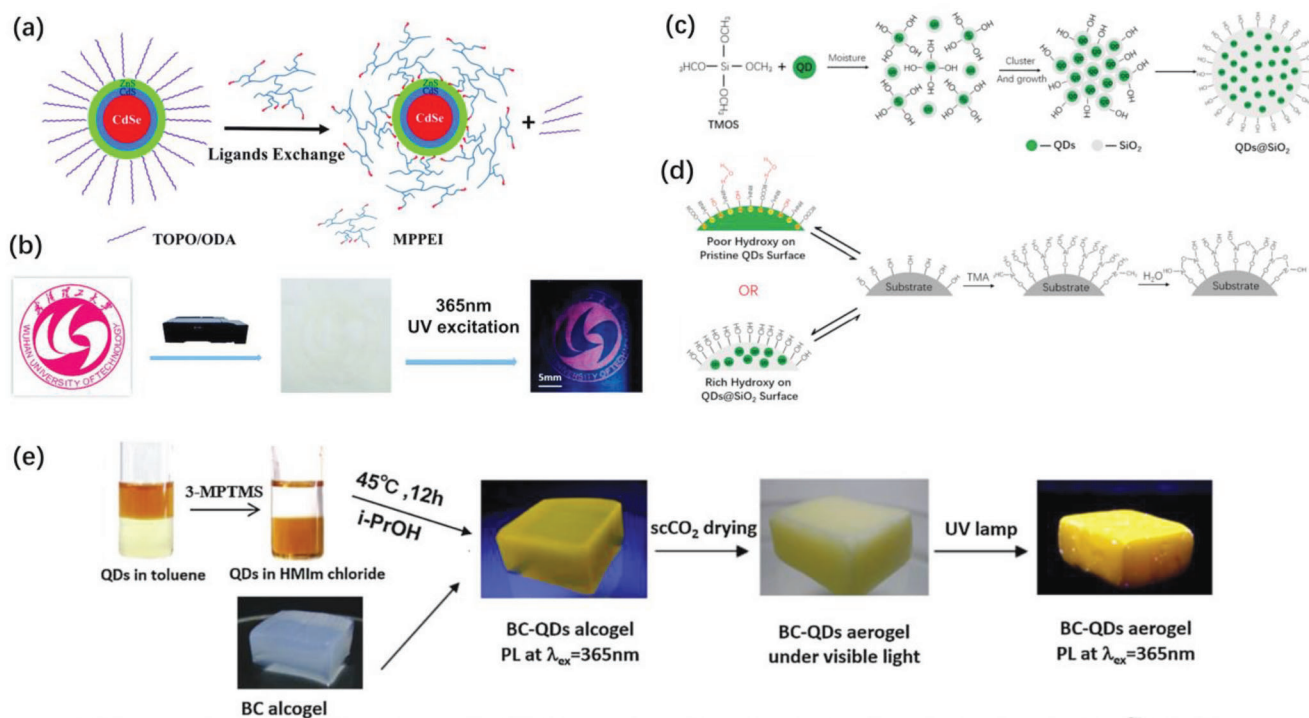


**Figure 3.** a) Synthetic route for preparing MPPEI-capped QDs. b) Inkjet printing process with MPPEI-capped QDs and photos of the printed pattern under ambient and UV light. Reproduced with permission.<sup>[75]</sup> Copyright 2013, Royal Society of Chemistry. c) Schematic of the reaction mechanism of the sol-gel method. d) Schematic of the ALD technique. Reproduced with permission.<sup>[76]</sup> Copyright 2020, Wiley-VCH. e) Preparation scheme for BC-templated ZnS(CuInS<sub>2</sub>)/ZnS QD aerogels. Reproduced with permission.<sup>[77]</sup> Copyright 2019, Elsevier Ltd.

solid-state matrix. Mechanical dispersion methods can be further divided into two types: mechanical dispersion without QD synthesis and mechanical dispersion with QD synthesis. The former employs ready-made QD dispersion for the mixture with matrix material, while the latter mixes precursors of QDs with the matrix material and then conducts the synthesis process of QDs. In addition, the physical dispersion method can also package QDs in crystals such as salts to improve their stability and performance. The resulting structures can be used directly or further encapsulated in polymers. Mechanical dispersion methods apply to most polymer and crystalline salt materials as packaging matrices.

Mechanical dispersion without QD synthesis is the most convenient strategy for packaging QDs. Mutlugun and co-workers synthesized high-quality green-, yellow-, and red-emitting CdSe/ZnS QDs and embedded them into a poly(methylmethacrylate) (PMMA) matrix using anisole and hexane solvents. Hybrid QD/PMMA films were obtained by drop-casting. The green, yellow, and red-emitting QD/PMMA films were characterized by emission peak wavelengths of 520, 562, and 626 nm, respectively, with FWHMs of 34, 35, and 26 nm, respectively, and PLQYs of 90%, 50%, and 78%, respectively. By combining green and red QD/PMMA films with blue LEDs, a high NTSC color gamut of 122.5 (CIE-1931) was achieved.<sup>[79]</sup> Similarly, the mechanical dispersion processes of PeQDs have been investigated. Kuo and co-workers used toluene and methylene chloride as intermediate solvents to prepare a mixture of CsPbBr<sub>3</sub> PeQDs with three commonly used polymers: poly(styrene-butadiene-styrene) (SBS), polystyrene (PS), and PMMA. Fiber network films were fabricated with

the obtained PeQD composites via electrospinning, as shown in **Figure 4a**. The CsPbBr<sub>3</sub>@SBS showed better compatibility, with uniform QD dispersion and the highest PLQY, while the CsPbBr<sub>3</sub>@PMMA film showed the most increased thermal stability owing to the high glass transition temperature of PMMA. The CsPbBr<sub>3</sub>@PS film exhibited the best water resistance, maintaining 83% of the PLQY value after three months of immersion in water. Furthermore, wrapped core-shell PeQD fiber films were prepared by a biaxial electrospinning method, which achieved a luminance and efficiency enhancement of more than 400% compared to multilayer-structured LED devices.<sup>[80]</sup>

Mechanical dispersion methods can also be used to disperse QDs in polymer materials and in various crystalline matrices. Because the crystalline matrix is more compact, better environmental stability, excellent optical properties, and better processability can be achieved. Gaponik and co-workers doped CdTe QDs into three conventional salt crystals (NaCl, KCl, and KBr) via saturated crystalline growth to form robust and strongly processable composites. These crystals could be further processed by directly mixing them into resins, such as PMMA, or other polymer matrices without performance degradation.<sup>[81]</sup> Based on these results, they also proposed a liquid-liquid diffusion-assisted crystallization (LLDC) method, as shown in **Figure 4b**, by utilizing the diffusion and solubility variation of inorganic salts in polar solvents to fabricate high-quality QD-salt hybrid crystals. Because the interdiffusion of poor solvents reduces the solubility of sodium chloride in water, complete crystallization was accomplished in less than a day, reducing the time required to produce mixed crystals by more than an order of magnitude. This

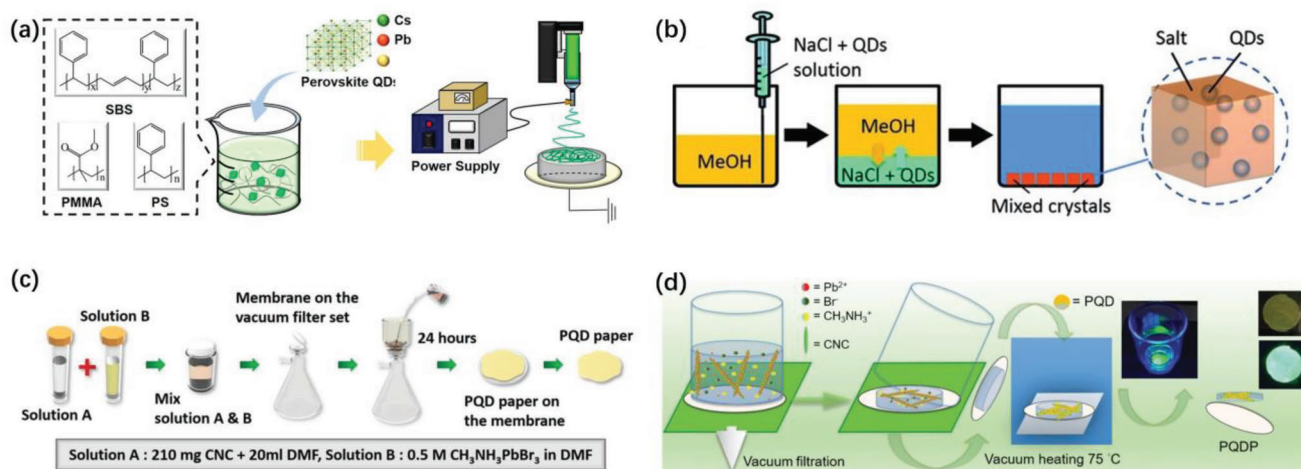


**Figure 4.** a) Schematic of the  $\text{CsPbX}_3$  ( $X = \text{Cl, Br, I}$ ) nanofiber fabrication process. Reproduced with permission.<sup>[80]</sup> Copyright 2019, The Authors, under the Creative Commons Attribution (CC BY) license. b) Illustration of the LLDC approach using the diffusion of MeOH through a stable interface layer into an aqueous solution containing NaCl and CdTe QDs. Reproduced with permission.<sup>[81]</sup> Copyright 2012, American Chemical Society. c) Fabrication process for PeQD paper. Reproduced with permission.<sup>[86]</sup> Copyright 2019, The Authors, published by Wiley-VCH. d) Flowchart of the preparation of UV-resistant PeQD paper using a vacuum filtration and chalcogenide growth method. Reproduced with permission.<sup>[87]</sup> Copyright 2020, The Authors, published by Wiley-VCH.

method was the first to achieve light emission by doping Cd-free QDs (e.g., InZnP/GaP/ZnS) into an ionic matrix. In addition, by extending the LLDC method to a two-step procedure, oil-based QDs were incorporated directly into ionic matrices without prior phase transfer.<sup>[82]</sup> Moreover, organic crystal matrices have also been investigated. Chen and co-workers incorporated MAPbBr<sub>3</sub> organic–inorganic hybrid PeQDs into carboxybenzene crystals in toluene by slow cooling to control the crystallization. The resulting needle-like hybrid microcrystals retained the high PLQY of PeQDs. Compared to PeQDs packaged in PS, the carboxybenzene crystals were more robust and better protected the PeQDs from moisture and photodegradation. This finding was attributed to the high compactness of the carboxyphenylene matrix. In addition, this versatile approach could preserve various QD materials besides organic–inorganic hybrid PeQDs, including all-inorganic PeQDs and chalcogenide QDs (e.g., CdSe/ZnS QDs and CuInS/ZnS QDs).<sup>[83]</sup>

In addition to the direct dispersion of synthesized QD materials into the solid-state matrix described above, methods combining the synthesis process of QD materials in the intermediate solvent and polymer environment are another option. These methods enable better dispersion of the QD materials in the matrix and are commonly used for PeQD materials. Chen and co-workers prepared CsPbBr<sub>3</sub> PeQD/ethylene vinyl acetate (EVA) composite films using a one-step method. The preparation process was as follows: the EVA polymer was first dissolved in toluene and rapidly mixed with a precursor solution consisting of PbBr<sub>2</sub>, CsBr, specific ligands, and the solvent DMF. The CsPbBr<sub>3</sub> PeQD was supersaturated and recrystallized during the natural drying process. Solidification of the EVA matrix occurred at the same time. The prepared composite films exhibited excellent performance with a color purity of 92% and a PLQY of 40.5%. Moreover, the prepared CsPbBr<sub>3</sub> PeQD/EVA films showed high flexibility and stability, maintaining an almost constant photoluminescence intensity after 1000 cycles of repeated bending.<sup>[84]</sup> Besides, Wang et al. proposed a novel swelling–deswelling microen-

capsulation method for fabricating stable and highly luminescent PeQD/polymer composite films. In this method, the precursors of PeQDs were first absorbed and confined in the polymer medium by a solvent-induced swelling process. Well-dispersed PeQDs were then synthesized in the polymer matrix after the solvent removal and the composite film was solidified as meanwhile. The obtained composite film showed a PLQY up to 48%.<sup>[85]</sup>

The strategy of incorporating QD synthesis into the packaging process can be applied to crystalline matrices as well. Kuo and co-workers proposed a novel solution for packaging CH<sub>3</sub>NH<sub>3</sub>PbBr<sub>3</sub> PeQDs in cellulose by adding cellulose nanocrystals into the PeQD precursor solution, followed by a ligand-assisted precipitation crystallization. This PeQD paper, a new type of QD film, exhibited high luminescence intensity peaking at 518 nm with an FWHM of 28 nm and optical absorption of 91%, as well as excellent stability owing to the complexation between nanocellulose and PeQDs. The fabrication process is illustrated in Figure 4c. The white LED consisting of this PeQD paper, red KSF phosphor, and a blue LED chip achieved a luminous efficiency of 124 lm W<sup>-1</sup>, NTSC color gamut of 123%, and viewing angle of 120°. The device exhibited good stability, with a luminescence decay of only 12.4% after 240 h of use.<sup>[86]</sup> He and co-workers introduced cellulose nanocrystals with a size on the order of 100 nm containing a large number of –HSO<sub>3</sub>– and –O– groups as long-chain binding ligands to stabilize the PeQD crystals without adding conventional ligands such as carboxylic acids and alkyl amines. A highly UV-stable PeQD paper was obtained via a vacuum filtration growth method, as shown in Figure 4d. The –HSO<sub>3</sub>– and –O– groups from the cellulose spatially restricted the growth of the PeQD crystals and eventually formed a well-dispersed PeQD paper. The entangled cellulose structure also formed an extra packaging for PeQDs, achieving excellent stability with ≈80% photoluminescence intensity remaining after eight months of exposure at 60% relative humidity and 20 °C, as well as ≈90% photoluminescence intensity remaining after 1000 h of continuous exposure to 16 W UV light.<sup>[87]</sup>

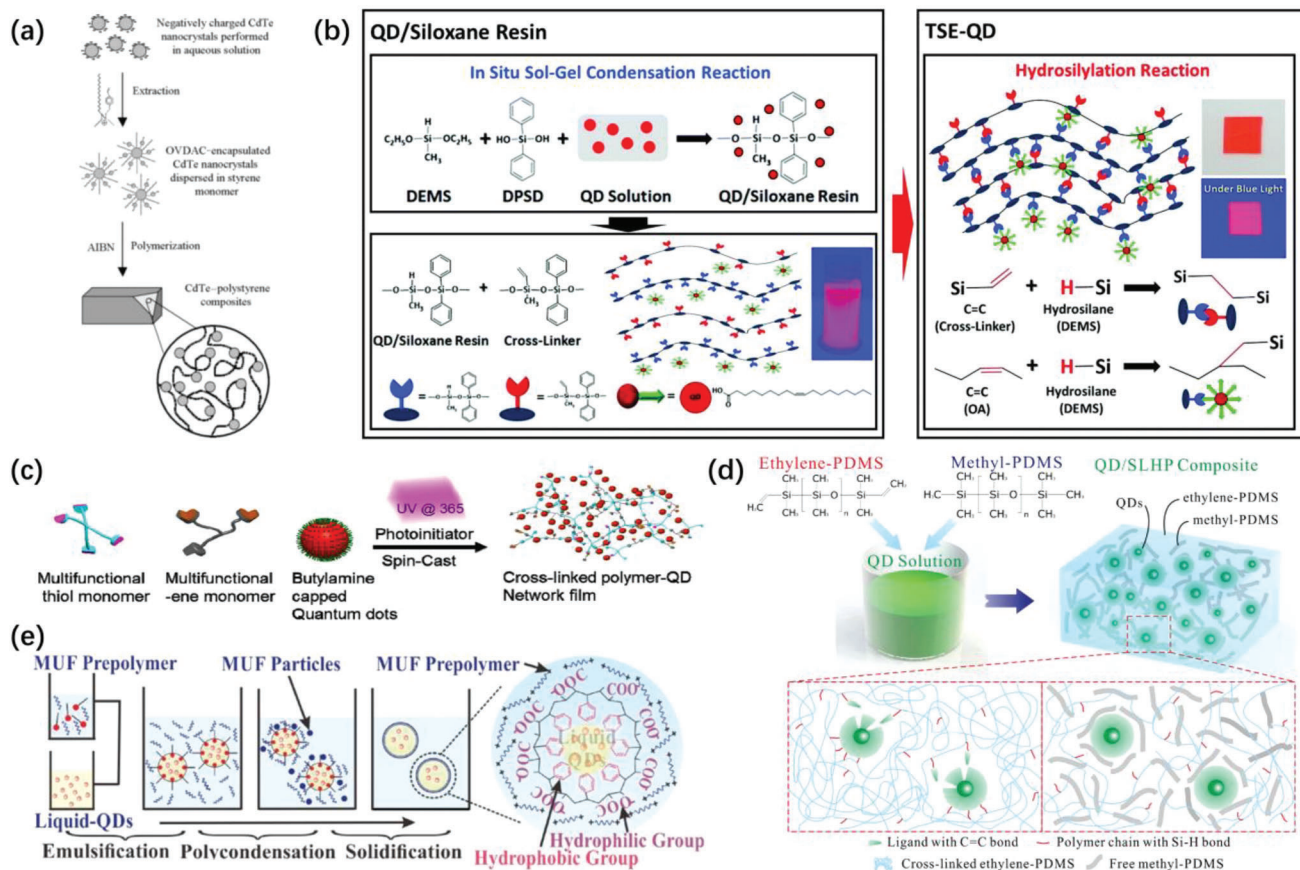


**Figure 5.** a) Procedure for the fabrication of fluorescent CdTe-PS composites. Reproduced with permission.<sup>[88]</sup> Copyright 2003, Wiley-VCH. b) Fabrication process for the TSE-QD film. Reproduced with permission.<sup>[89]</sup> Copyright 2017, Society for Information Display. c) Mechanism for the fabrication of NOA-BAQD composites. Reproduced with permission.<sup>[92]</sup> Copyright 2017, American Chemical Society. d) Fabrication method for QD/SLHP composites. Reproduced with permission.<sup>[93]</sup> Copyright 2018, Optica Society. e) Schematic of the liquid-QD/MUF microcapsules fabricated via in situ polymerization. Reproduced with permission.<sup>[95]</sup> Copyright 2021, IEEE.

### 3.3. In Situ Polymerization

The principle of in situ polymerization is to embed QD materials into polymers directly in situ, i.e., the precursor of the polymer and the QDs are homogeneously mixed first, then polymerization of the monomers is carried out to form the solid-state QD/polymer composite.

Gao and co-workers used polymerizable octadecyl p-vinylbenzyl dimethyl ammonium chloride as a surfactant to transfer CdTe QD aqueous solutions with bright photoluminescence into styrene monomer solutions. Subsequently, transparent CdTe/PS bulk composites were obtained through the polymerization reaction of styrene monomers, as shown in **Figure 5a**. This method is not only applicable to PS polymers but also to other common polymers formed by radical polymerization such as PMMA.<sup>[88]</sup> This method is straightforward and convenient for creating composites of aqueous synthetic QD materials with polymers. Lee and co-workers synthesized and compared the properties of two different (CdSe/ZnS) core-shell QD/siloxane composite films, one of which was a QD/siloxane (methacrylic acid) film with bonding between the QDs and siloxane, and the other of which was a QD/siloxane (epoxy) film

without bonding between the QDs and siloxane. The former was obtained through a free radical addition reaction, while the latter was prepared through an epoxide ring-opening reaction; both reactions were driven by UV light. These methods are based on the hydrophobic interactions between oleic acid on the QD surface and the siloxane matrix's functional groups, enabling the homogeneous dispersion of the QDs. Owing to the cross-linked bonds between the oleic acid and the methacrylic acid groups of the siloxane matrix, the PLQY of the QD/siloxane (methacrylic acid) film did not decrease in environments of 85 °C/5% relative humidity (RH) or 85 °C/85% RH. By contrast, the PLQY of the QD/siloxane (epoxy) film was severely reduced.<sup>[89]</sup>

Moreover, Bae and co-workers reported a thermally curable QD/siloxane hybrid (TSE-QD) color converter with excellent stability, even under high temperature and high humidity. **Figure 5b** shows that the TSE-QD color converter was prepared by dispersing the in situ sol-gel-synthesized QDs in a siloxane resin (QD/siloxane resin) without additional ligand-exchange processes, followed by a thermally induced hydrosilylation reaction. Using this method, the QDs were uniformly distributed within the siloxane matrix, thereby maintaining their original optical properties. Based on a yellow TSE-QD color converter, a

white LED was established by directly combining it with a blue LED chip. The device exhibited excellent spectral stability, outstanding reliability at 85 °C/85% RH, and a wide color gamut (116% NTSC).<sup>[90]</sup> Based on this strategy, they developed a thermally stable and photostable QD-embedded silica/siloxane (S-QD/siloxane) film via a two-step sol-gel reaction. To fabricate the composite film, QDs were first embedded into silica with tetraethyl orthosilicate assistance. Then the QD-embedded silica was homogeneously dispersed in oligo-siloxane resin by sol-gel condensation. The composite film did not agglomerate even at QD concentrations of up to 5 wt%. In addition, it showed excellent heat, moisture, and chemical stability compared to oleic acid-capped QD/siloxane films because of the presence of the two-step barrier of silica and siloxane.<sup>[91]</sup>

In addition, thiol-ene chemical photopolymerization is another classical strategy for fabricating composite QD materials with polymers. Because the polymerization is excited by UV light, which enables integration with lithography, this method is suitable for patterning QD materials and has broad applicability for various processes. Tsukruk and co-workers prepared highly loaded nanocomposite films by compounding butylamine-capped CdSe/Cd<sub>1-x</sub>Zn<sub>x</sub>Se<sub>1-y</sub>S<sub>y</sub> QDs (BAQDs) with high stability using UV-curing by a thiol-ene chemical photopolymerization reaction. A schematic representation of the packaging method is shown in Figure 5c. In BAQDs, only amine functional groups are present on the surface of the QDs, which will not affect photopolymerization. Moreover, the rapid UV polymerization generates massive cross-linked polymer networks that inhibit the aggregation of QDs, resulting in a better capability for high QD loading up to 30 wt%. The composite exhibited good flexibility, elasticity, and tuneable mechanical and thermal properties owing to the controllable cross-linking while maintaining excellent optical performance. The composite films were also compatible with nanoimprinting techniques.<sup>[92]</sup>

In addition to the solid-state composites mentioned above, because QD materials generally show better optical performance in liquid environments, many reports have focused on the solid-liquid hybrid packaging and liquid-type packaging of QD materials. Li et al. proposed an efficient QD-enhanced LED with solid-liquid packaging using solid-liquid hybrid polydimethylsiloxane (PDMS) as the dispersion matrix, as shown in Figure 5d. Ethylene-PDMS and methyl-PDMS were utilized in this method. After thermal treatment, the ethylene-PDMS interacted with the curing agent and formed a solid-state cross-linked network, while the methyl-PDMS remained in the liquid state and was packaged in the solid network. Macroscopically, the QD/solid-liquid hybrid PDMS (SLHP) composite film remained solid, but microscopically, a liquid environment was present inside to enable the dispersion of the QDs and inhibit surface defects. When the concentration of methyl-PDMS was 85 wt%, which was the maximum concentration at which the ethylene-PDMS could be fully cross-linked and remained in the solid-state, the LEDs packaged with this QD/SLHP composite showed a 13.0% enhancement in the luminous flux. Furthermore, the luminous flux maintenance under harsh aging conditions was comparable to ordinary solid QD/PDMS composites.<sup>[93]</sup> They also proposed a methyl-terminated PDMS-based liquid-type packaging structure to improve the stability and optical performance of QD-based LEDs. Compared with the

solid-type packaging structure at the same QD contribution to the emission of 80%, the initial total radiant power, and luminous flux were increased by 23.2% and 26.1%, respectively.<sup>[94]</sup> Microcapsule packaging is a liquid-type packaging method for QDs. As shown in Figure 5e, liquid-QD/melamine-modified urea-formaldehyde (MUF) microcapsules were fabricated using liquid-QDs with chlorobenzene and MUF as the core and shell structures, respectively. The microcapsules demonstrated an increase in the luminous efficiency of 15.9% compared to the traditional solid QDs at a specific QD energy proportion.<sup>[95]</sup>

In addition to Cd-based QD materials, in situ polymerization strategies are also widely used to fabricate composites with PeQD materials. Because of their poor stability and good solution processability, PeQDs are commonly encapsulated in polymer matrices. Yu and co-workers proposed a novel alkoxy-silane-assisted one-pot synthesis and hydrolysis method, which homogeneously synthesizes and disperses CsPbX<sub>3</sub> PeQDs into silicone matrices by controlling the amount of oleic acid and APTES ligands. PeQD gels with high transparency, flexibility, and PLQY were obtained using this method. Compared to the usual solvent evaporation method, because the octadecene ligand is nonvolatile, the PeQD gel can retain its original shape after curing without shrinkage or matrix collapse. Moreover, the stability of the PeQD gel was greatly improved due to the silica network's excellent protection and the alkoxy-silane's passivation. The PLQY of the red PeQD gel reached 35%. A white LED device was realized by packaging red and green PeQD gels with blue LED chips, achieving an NTSC color gamut of 128%.<sup>[96]</sup>

Considerable research has focused on packaging methods for QDs, but these methods are still far from mature commercial applications. For example, many methods mentioned above use toxic organic solvents such as toluene and methylene chloride, which harm humans and the environment. In particular, mechanical dispersion methods rely heavily on organic solvents, and in situ polymerization methods often require organic solvents as the reaction environment. Surface modification methods that use functional groups on the surface of the QDs to modify their properties for better packaging require a more demanding synthesis of QD materials and are more complex than the other two methods. In addition, there is still much room for improvement in PLQY value for the three strategies above, as the problem of ligand debonding commonly happens in solid-state packaging. Maintaining the excellent optical properties of QD and simultaneously protecting them to obtain better stability through a simple, low-cost, highly repeatable, and green process is the direction of future research and the key to promoting QD materials for large-scale commercial applications.

#### 4. Light Management of QD Composites

The PLQY, luminescence stability, chemical stability, thermal stability, and other properties of QD composites need to be further improved to meet the requirements for commercial applications such as mini/micro-LED displays. Besides developing solid-state packaging methods for QD materials, the introduction of appropriate microstructures or micropatterns to QD composites can enhance their optical performance. Higher photoluminescence intensity can be achieved through enhanced optical outcoupling

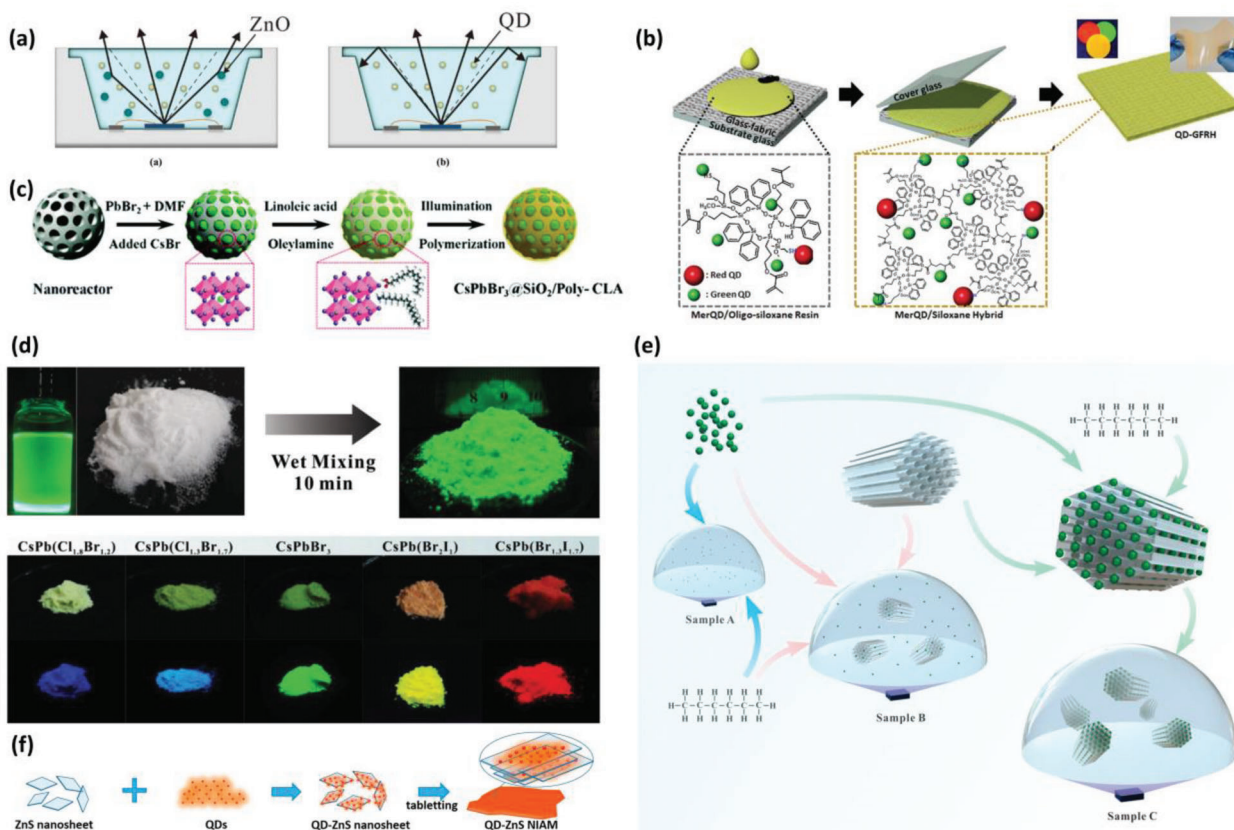


**Figure 6.** a) Schematic cross-sectional view of a ZnO-incorporated QD-converted LED. Reproduced with permission.<sup>[100]</sup> Copyright 2018, IEEE. b) Fabrication procedure for a QD-GFRH film through vacuum bag pressing and UV radiation as well as the molecular structure of the 3-mercaptopropylmethyldimethoxysilane-passivated QD/oligosiloxane resin and siloxane hybrid. Reproduced with permission.<sup>[104]</sup> Copyright 2020, Wiley-VCH. c) Schematic illustration of the formation of CsPbBr<sub>3</sub>@SiO<sub>2</sub>/poly-conjugated linoleic acid. Reproduced with permission.<sup>[107]</sup> Copyright 2021, Royal Society of Chemistry. d) Photographs of CsPbBr<sub>3</sub>/hexane PeQD solution, S-AIM powders, and green AeroPeQD powders obtained by wet-mixing (first row). Photographs of AeroPeQD powders with different colors (blue, cyan, green, yellow, and red) under sunlight illumination (second row) and UV light illumination (third row). Reproduced with permission.<sup>[108]</sup> Copyright 2020, Wiley-VCH. e) Fabrication of the QD/SBA-15/silicon composite (sample C). As references, fabrications of QD/silicon composite without SBA-15 (sample A) and QD/SBA-15/silicon composite with direct mixing of SBA-15 (sample B) are illustrated as well. Reproduced with permission.<sup>[111]</sup> Copyright 2021, American Chemical Society. f) Illustration of the preparation procedure for the QD-ZnS nanosheet inorganic assembly monolith. Reproduced with permission.<sup>[112]</sup> Copyright 2017, The Authors, under an open access Creative Commons CC BY 4.0 license.

or and better stabilities can be realized with a hydrophobic surface texture. With the introduction of microstructures or micropatterns, a lower concentration of QDs is required to obtain the same photoluminescence intensity, reducing QD light reabsorption events. Reabsorption loss is a significant factor that decreases the efficiency of QD color converters.<sup>[97–99]</sup> Here, we divide the relevant studies into three categories: internal scatterers, internal porous structures, and surface structures.

#### 4.1. Internal Scatterers

The use of internal scatterers for improving QD composites can be further divided into direct and indirect methods. The former involves directly packaging a new medium, such as scattering powder into the solid-state matrix. By contrast, the latter uses porous materials such as mesoporous SiO<sub>2</sub> to adsorb the QDs, followed by packaging the obtained composite material in the packaging matrix.

##### 4.1.1. Direct Scatterer Methods

Direct scatterers make use of the scattering effect by the embedded materials. This increases the optical path of excitation light inside a QD composite through multiple scattering, thus increasing the probability of the QD materials being excited by the blue or UV radiation and improving the color conversion efficiency. Li and co-workers embedded many types of particles in QD composites to enhance their optical properties. Due to the strong scattering, ZnO particles were selected and introduced into QD-converted LEDs. The schematic of the QD-converted LEDs with and without ZnO particles in **Figure 6a** shows that the scattering effect improved the utilization of blue light and the outcoupling of the emitted light. However, they also found that the total radiant flux of the LEDs decreased with excessive ZnO nanoparticle doping because the excessive ZnO particles saturated the enhancement of the absorption of QDs. By contrast, the backscattering of the ZnO particles led to a significant loss of luminescence. After optimization, a luminous flux enhancement of

3.37% was obtained when the QD-converted LEDs contained 0.1 wt% ZnO particles. Compared to conventional devices, the LEDs maintained a similar color coordinate and reduced the angle-dependent correlative color temperature deviation from 862 to 712 K in the angular range of  $-70^\circ$  to  $70^\circ$ .<sup>[100]</sup> Moreover, they further exploited the scattering property of SiO<sub>2</sub> particles and introduced them into hemispherical lenses of QD/PDMS to realize white LEDs at a concentration of 0.1 wt%, which increased the color conversion efficiency of the QDs. Furthermore, it provided enhancements of the radiant efficiency of 5.04% and the luminous efficiency of 11.08%, respectively.<sup>[101]</sup> Similarly, they packaged carbon dot LEDs with silicone and introduced TiO<sub>2</sub> particles to enhance scattering. Because the TiO<sub>2</sub> particles could increase the excitation and extraction probability. The luminous intensity could be increased by 31% at a TiO<sub>2</sub> particle concentration of 0.05 wt%.<sup>[102]</sup>

Based on a similar scattering mechanism, Theobald et al. proposed a new design for a selective reflector based on scattering core-shell nanoparticles to address two problems of QD composites: the limited absorption of excitation light and the poor out-coupling of downshifted photons. By optimizing the light scattering properties of the single core-shell nanoparticles at the corresponding excitation and emission wavelengths, as well as tuning the spatially dependent concentrations of the nanoparticles, a fourfold enhancement in UV light absorption and a twofold increase in coupling efficiency were shown based as compared to the reference layout comprising of a distributed Bragg reflectors atop the conversion layer.<sup>[103]</sup>

In addition to the introduction of scattering particles into QD/polymer composites, a new process for embedding glass fibers into QD/polymer composites was designed by Bae and co-workers. By impregnating thermally and chemically stable QD/siloxane resins into porous glass fibers, a QD-embedded glass-fiber-reinforced siloxane hybrid (QD-GFRH) composite with a high haze value and high stability was fabricated. The fabrication process is illustrated in Figure 6b. The haze value of the composite can be easily adjusted based on the refractive index mismatch between the siloxane resin matrix and the glass fibers. This approach can effectively improve the light extraction of the QD-GFRH composite. The hazy QD-GFRH composite showed a twofold improvement in photoluminescence extraction, improvements in various mechanical properties such as thermal expansion, and high deformation resistance. In addition, as the QDs were chemically dispersed inside the composite by covalent cross-linking with the siloxane matrix, the QD-GFRH composite exhibited long-term stability under high temperature (85 °C) and high humidity (85% RH) conditions.<sup>[104]</sup>

The direct introduction of scatterers is relatively simple and effective. However, the enhancement relies on a compromise of enhanced excitation and outcoupling on the one hand, and increased backscattering on the other hand. Excessive concentrations usually reduce the device's overall efficiency, which limits the application prospects of these methods.

#### 4.1.2. Indirect Scatterer Methods

When using indirect scatterer methods, first a composite material using porous materials such as mesoporous silica is used to

adsorb the QDs, followed by packaging the composite in a solid-state matrix. In addition to enhancing the photoluminescence intensity and conversion efficiency, these methods can improve the dispersibility, thermal stability, lifetime, and other properties of QD materials.

Liu and co-workers introduced mesoporous silica materials into the QD packaging process to eliminate the broadening of the QD emission peak caused by ion exchange that occurs when incorporating QD materials into a polymer matrix. The mesoporous material was used to adsorb green and red PeQDs to form a composite material which was then dispersed in silicone resin and packaged resulting in a blue LED pumped emitter for the backlighting of displays. The WLEDs exhibited a wide color gamut, reaching 113% NTSC and 85% Rec. 2020.<sup>[105]</sup> Based on these results, they proposed a three-step treatment of CsPbBr<sub>3</sub> QDs, including introducing an inorganic-organic hybrid ion pair (didodecyl dimethylammonium sulfide, S<sup>2-</sup>-DDA<sup>+</sup>) to passivate the surface defects of PeQDs to improve the PLQY, along with coating the mesoporous CsPbBr<sub>3</sub> composites with a polymer matrix to obtain mesoporous CsPbBr<sub>3</sub>/SDDA@PMMA powder. The obtained powder achieved a high PLQY of 63% and exhibited good luminescence stability, dispersibility, and water resistance. This result can facilitate the use of PeQDs for color conversion applications in a way similar to traditional phosphors. WLEDs were produced by mixing the obtained powder with a red-emitting K<sub>2</sub>SiF<sub>6</sub>:Mn<sup>4+</sup> phosphor and then pumped by a blue LED chip. They achieved a color coordinate of (0.271, 0.232) and an NTSC color gamut of 102%.<sup>[106]</sup> Similarly, Li and co-workers successfully prepared CsPbBr<sub>3</sub> QDs grown in situ in a mesoporous silica microsphere template with conjugated linoleic acid as the ligand for the QDs, as shown in Figure 6c. Moreover, the synthesized QDs could be used as photoinitiators to initiate the polymerization of conjugated linoleic acid to form a hydrophobic polymer coating on the surface of mesoporous silica microspheres to achieve higher stability. The mesoporous silica microsphere template limited the growth and agglomeration of the CsPbBr<sub>3</sub> QDs through spatial confinement, resulting in a narrow FWHM of 20 nm and a high PLQY of 79.16%. In addition, because of the protection by the hydrophobic polymer coating, the improved water resistance of the CsPbBr<sub>3</sub> QDs allows for the retention of 77% of their photoluminescence intensity after soaking in water for a week.<sup>[107]</sup>

Li et al. used a superhydrophobic aerogel inorganic matrix (S-AIM) for the postabsorption of PeQDs to prepare superhydrophobic so-called AeroPeQDs. The configuration and structure of the obtained AeroPeQDs are shown in Figure 6d. The aerogel matrix not only enhanced the water resistance of the PeQDs but also enabled new functions, such as the ability to bond with Fe<sub>3</sub>O<sub>4</sub> nanoparticles to obtain magnetic properties. The proposed superhydrophobic AeroPeQDs maintained a high PLQY of 75.6% after being embedded into the aerogel matrix, whereas the original PeQD material showed a PLQY of 83.2%. The excellent optical performance was attributed to the lipophilic functional groups of S-AIM and its suitable pore size, which acted as good dispersion templates for PeQDs during solvent evaporation and suppressed aggregation and surface defects. Moreover, the AeroPeQDs exhibited excellent stability and water resistance. After 3.5 months of complete immersion in water, the AeroPeQDs still maintained a PLQY of 50.5%. Moreover, its photoluminescence intensity

barely decreased in the first 11 d, whereas the conventional PeQDs quenched within one day of immersion. The excellent water resistance of AeroPeQDs is due to the matching size between the pores and particles, the surface lipophilic functional groups, and the rough surface of the S-AIM. In addition, the AeroPeQDs retained 50% of their photoluminescence intensity after 49 h of aging (thereof 24 h under UV irradiation). In comparison, ordinary the efficiency of PeQD materials decreased dramatically to less than 20% after this treatment. From an application perspective, the luminous efficiency of the AeroPeQD WLED ( $59.8 \text{ lm W}^{-1}$ ) was 11.8% higher than that of the WLED using conventional PeQD material owing to the scattering effect of S-AIM, which enhanced the overall photoluminescence intensity.<sup>[108]</sup> In addition, SBA-15 mesoporous particles with a unique 2D hexagonal pore structure (2D-HPS) were used for the silicone packaging of QD materials. The 2D-HPS of SBA-15 could adsorb and package QDs and generate a waveguide effect, which reduced the reabsorption loss of the QD materials by confining and extracting the emitting light through the 2D-HPS frame. Compared with the WLEDs packaged with ordinary QD/silicon composites, WLEDs incorporating the QD/SBA-15/silicon composite achieved a luminous efficiency and color conversion efficiency improvement of more than 50% and a 1.9-fold increase in lifetime under harsh aging conditions.<sup>[109,110]</sup> Moreover, as shown in Figure 6e, three configurations of QD-converted LEDs, including direct embedding of QDs (sample A), direct embedding of QDs and SBA-15 nanoparticles (sample B), and the embedding of QD-mixed SBA-15 nanoparticles (sample C), were investigated. By further optimizing the packaging methods and the introduced nanocomposite particle mass ratio, highly efficient QD WLEDs with wet-mixed QD/SBA-15 nanoparticles were obtained. The LEDs demonstrated a record luminous efficacy (the ratio of luminous flux to electrical power) of  $206.8 \text{ lm W}^{-1}$  (entrusted test efficiency of  $205.8 \text{ lm W}^{-1}$  certified by the China National Accreditation Service) and  $137.6 \text{ lm W}^{-1}$  at 20 mA for WLEDs integrating only green QDs and green–red QD color converters, respectively, with improved operating stability.<sup>[111]</sup>

To address the problem of thermally induced luminescence quenching of QD materials, Bi and co-workers incorporated QD materials with ZnS nanosheets synthesized through a low-temperature hydrothermal route via a monodisperse chemisorption method and pressing process to obtain a QD-ZnS nanosheet inorganic assembly (NIAM), as shown in Figure 6f. This NIAM could be directly mounted on an LED chip as a color converter, reducing the thermally induced luminescence quenching and enhancing the optical and chemical stability. As a result, the QD converter could maintain more than 90% of its initial brightness when the operating temperature reached  $85 \text{ }^\circ\text{C}$ .<sup>[112]</sup>

## 4.2. Internal Porous Structure

The enhancement mechanism of the internal porous structure is similar to that of the direct doping structure but relies on different implementation methods. Generally, this strategy improves the efficiency of QD materials by creating micropores or microholes as scattering mediums inside the QD color conversion composite to increase the absorption of excitation light and enhance light extraction. Yu and co-workers introduced a supercrit-

ical  $\text{CO}_2$  foaming technology to form a microporous structure in a PMMA composite film embedded with CdSe/ZnS QDs, which significantly enhanced the overall photoluminescence intensity of the QD-based color conversion film compared to the composite without a porous structure. A schematic of the foaming process is shown in Figure 7a. The microporosity increased the angular spread of the UV/blue excitation inside the polymer matrix. The optical scattering stems from the refractive index contrast between the microvoids and the polymer matrix. This approach nevertheless maintains a high transmittance of up to 80% in the visible range. For the porous network, a maximum photoluminescence intensity enhancement factor of 6.6 was measured compared to the QD/PMMA composite film without foaming. Furthermore, ray-tracing simulations confirmed that this enhancement is partly caused by the extended optical path length of the exciting UV/blue photons in the conversion medium. This leads to increased absorption by the QD material. In addition, the PLQY of the QD composite was simultaneously enhanced, as the porous network provided a better light extraction than the planar nonfoamed composite and reduced the reabsorption effect. This method was shown to be adequate for a wide range of QD concentrations until the concentration saturated the absorption of excitation light by the QD composite.<sup>[113]</sup> Recently, they demonstrated a polymerization-induced phase separation method for fabricating porous structures on a nanoscale, which exhibits excellent scattering properties. By incorporating the obtained nanoporous film as a back reflector into a QD-converted chip-on-board LED device, an optical power enhancement of 20% was measured under the driving current of 150 mA.<sup>[114]</sup>

Jung and co-workers proposed a QD composite film assembled with a poly-(styrene-*b*-4-vinylpyridine) (PS-*b*-P4VP) block copolymer (BCP) in addition to internal microstructures using a phase separation method. As shown in Figure 7b, multiscale phase separation features were generated by controlling the humidity, including micrometer-scale spinodal decomposition between the polymer-rich and water-rich phases as well as sub-10-nm-scale phase separation between the polymer blocks. The QD-BCP composite film with a random porous structure exhibited a significant improvement in both light absorption and extraction efficiency owing to the scattering property of the porous structure. In addition, the porous morphology substantially reduced the Förster resonance energy transfer efficiency from 53% to 22%. They achieved a 21-fold enhancement in the photoluminescence intensity for the QD-BCP composite film compared to the pure QD film.<sup>[115]</sup>

In addition to these two phase-separation methods for fabricating microporous structures inside the matrix, Kang et al. applied a conductivity-dependent electrochemical etching process to prepare nanoporous GaN to improve the color downconversion of micro-LEDs. Many nanoporous holes were first etched on the GaN material, and colloidal QD material was loaded into the hole structure as a color converter. The design of the nanoporous system and the related equipment are shown in Figure 7c. The measured transport mean free path (TMFP) in nanoporous GaN was 660 nm for a light wavelength of 450 nm and decreased with decreasing light wavelength. With shorter TMFP, the light extinction coefficient of the nanoporous GaN material at 370 nm was increased 11-fold. Enhanced by the multiple light scatterings inside the porous structure, the loaded QD materials exhibited a

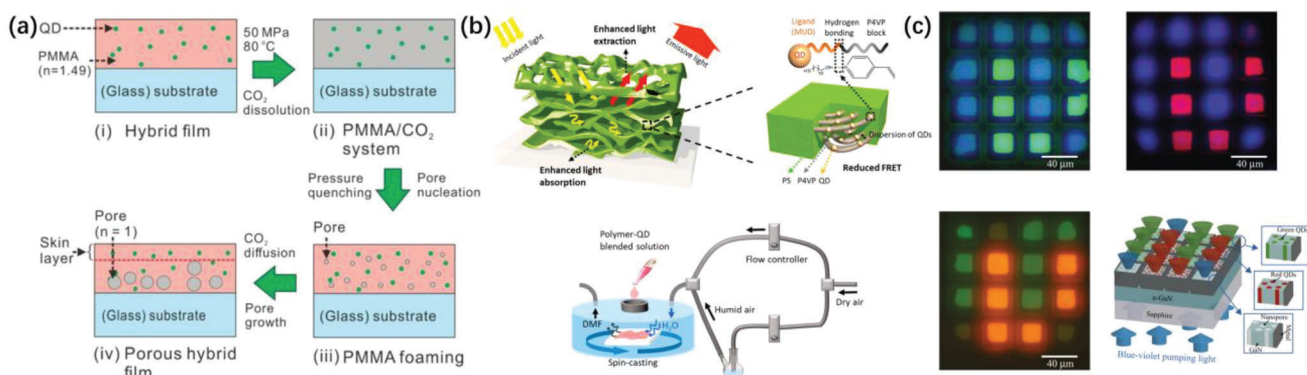


**Figure 7.** a) Schematic of the supercritical CO<sub>2</sub> foaming approach for QD/PMMA hybrid film. Reproduced with permission.<sup>[113]</sup> Copyright 2019, Wiley-VCH. b) Illustration of a randomly porous BCP-QD film at sub-micrometer and sub-10-nm scales, as well as the humidity-controlled spin-casting equipment. Reproduced with permission.<sup>[115]</sup> Copyright 2019, American Chemical Society. c) Optical microscope images of the multicolor arrays with a blue-violet pumping light and schematics of the structures of nanoporous GaN structures. Reproduced with permission.<sup>[116]</sup> Copyright 2020, American Chemical Society.

significant improvement in absorption. They achieved a surprisingly high 96% and 100% light conversion efficiencies for green and red emissions, respectively.<sup>[116]</sup>

### 4.3. Surface Structure

The surface structure strategy involves attaching an additional functional layer, or directly fabricating a surface texture on the micro/nanoscale, on the surface of the QD composite. The enhancement mechanisms of surface structures include the scattering effect of the texture, the wavelength-dependent reflection and transmission spectra of the functional layer, and the plasmonic effect of metal nanoparticles.

Ma and co-workers utilized Ag nanoparticle layers with single or double surface plasmon resonances (SPRs) prepared using a layer-by-layer assembly approach to enhance the photoluminescence intensity of PbS QD composites under different excitation wavelengths. By adjusting the excitation wavelength and the overlap between the SPR band of the Ag nanostructure and the emission band of the QD material, a maximum photoluminescence enhancement factor of 2.8 was achieved.<sup>[117]</sup> Similarly, Yang and co-workers compounded silica-coated Au nanoparticles/nanorods as fluorescence-enhancing structures with a QD/poly(diallyl dimethylammonium chloride) (PDDA) composite using an electrostatic self-assembly technique. The configuration of the Au-enhanced QD composites is shown in **Figure 8a**. By optimizing the size of the Au nanoparticles and the thickness of the silica coating, 17.8-fold and 24.7-fold fluorescence enhancements were obtained for silica-coated Au nanoparticles and nanorods, respectively.<sup>[118]</sup> In addition, Basu and co-workers applied the Langmuir–Blodgett method to prepare a compact QD monolayer and used a dip-coating method to cap a partially aligned gold nanorod array on top of the QD monolayer in close proximity. The resulting structure achieved a photoluminescence intensity enhancement factor of up to  $\approx 11$  and increased the photoluminescence anisotropy to 0.9.<sup>[119]</sup>

Inspired by nature, Li and co-workers proposed a microcavity cone array (MCA) composite mimicking the surface texture of the wings of the phoenix butterfly and incorporated it with a QD composite to obtain single-sided microstructured QD (SSM-QD) and double-sided microstructured QD (DSM-QD) composites, as shown in **Figure 8b,c**, to improve the color conversion efficiency (CCE) of QD-LEDs. Based on optical simulations, the diameter, aspect ratio, and pitch of the MCAs were optimized to 2.8 μm, 0.5, and 3 μm, respectively. In addition, the MCA composite exhibited higher reflectance and lower transmittance values (21% and 75%, respectively) when the light impinged from the plane side compared to the situation with the light impinging from the textured side (5% and 95%, respectively). As a result, the CCEs of the LED devices incorporating the SSM-QD and DSM-QD composites increased from 19.98% to 21.59% and 21.78%, respectively, with a driving current of 350 mA. This enhancement was attributed to the scattering effect of the MCA composite, which increased the light path of the excitation light, and the reflection effect, which helped to extract the backward emission light of the QDs.<sup>[120]</sup> A blue antitransmission film (BATF) was also introduced to improve the CCE and stability of QD composites. The CCE could be increased by as much as 93% using 15 layers of BATFs for the same QD concentration. In addition, the hybrid composite could effectively suppress the redshift of the QD light spectra and the expansion of the FWHM.<sup>[121]</sup> BN nanoparticles were also used as the reflective layer in inverted QD-LEDs to improve their performance. The color conversion probability was increased using the optimized concave BN-incorporated reflector structure. The luminous flux was increased by as much as 82.8% compared to that of conventional inverted QD-LEDs.<sup>[122]</sup> PS fiber films can also be used as a reflective layer to enhance luminous efficiency. Fabricating a microfiber-silicone hybrid structure by electrospinning increased the luminous efficiency by 31.7%.<sup>[123]</sup> For the first time, a uniform electrical induction technique was introduced to fabricate a sandwich column array structure (SCAS) for QD composites. The fabrication process is shown in **Figure 8d**. Because of the microcavity trapping and light extraction effects, the SCAS significantly

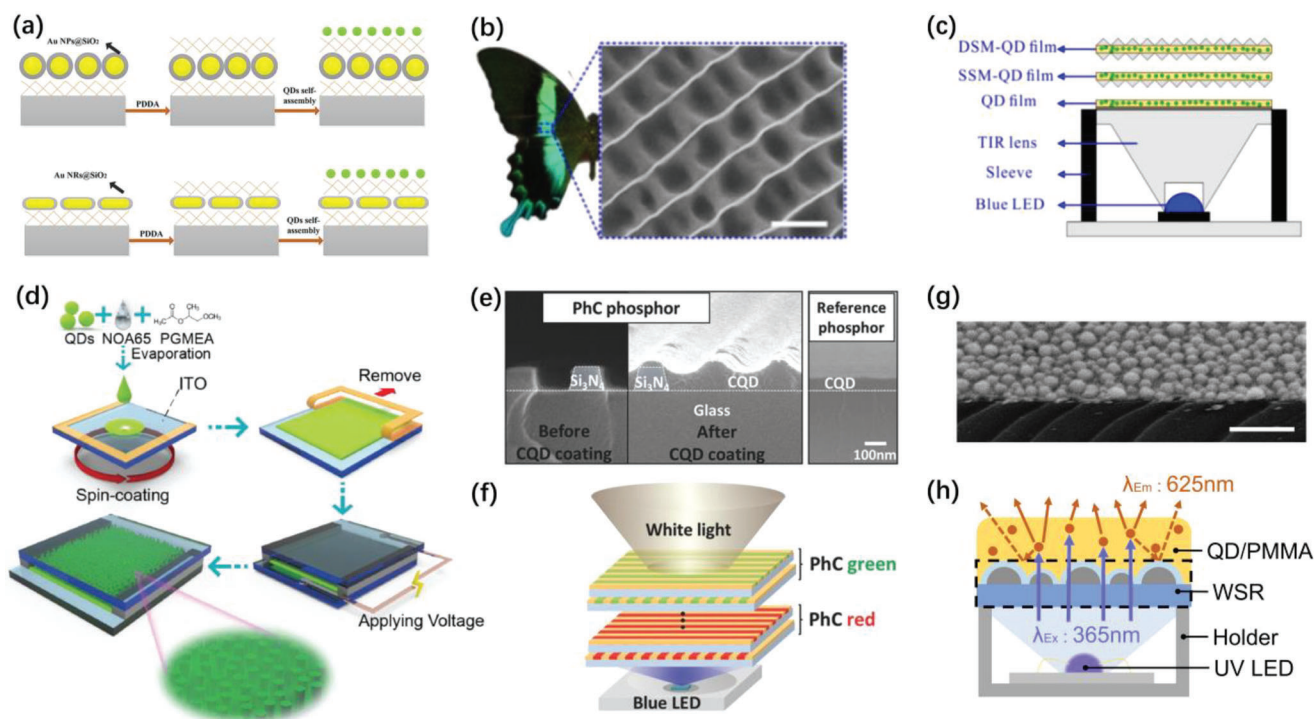


**Figure 8.** a) Schematic illustrating the assembly of CdSe@ZnS QDs on gold nanoparticles and gold nanorods. Reproduced with permission.<sup>[118]</sup> Copyright 2019, Elsevier B. V. b) *Papilio blumei* butterfly and the microconcave cone array of its wings (scale bar: 10  $\mu\text{m}$ ). c) Schematic of LED devices with QD, SSM-QD, and DSM-QD films. Reproduced with permission.<sup>[119]</sup> Copyright 2016, Springer Nature. d) Schematic of the fabrication of an SCAS-QD film by electrical induction. Reproduced with permission.<sup>[124]</sup> Copyright 2021, IEEE. e) Cross-sectional SEM images of the PhC phosphor before and after CQD coating (left) and the reference phosphor (right). f) Schematic of the device assembly for white light generation. Reproduced with permission.<sup>[125]</sup> Copyright 2017, Wiley-VCH. g) Cross-sectional SEM image of a WSR taken with a tilted angle of 60°, the scale bar represents 400 nm. h) Illustration of the operational principle of a WSR integrated within a UV-pumped LED with QD color conversion film. Reproduced with permission.<sup>[126]</sup> Copyright 2021, The Authors, published by American Chemical Society.

enhanced the photoluminescence intensity by 42.8% at the same QD concentration.<sup>[124]</sup>

Jeon and co-workers proposed a structurally engineered QD phosphor based on 1D photonic crystals (PhCs) consisting of silicon nitride as the high-index medium and dense colloidal QDs as the fluorescing low-index material. To obtain the desired PhC structure, they first deposited a 90-nm-thick  $\text{Si}_3\text{N}_4$  composite on a borosilicate glass substrate by plasma-enhanced chemical vapor deposition and fabricated a grating structure via photolithography and reactive ion etching. Subsequently, the CdSe colloidal QDs were spin-coated on the PhC structure. The details of the design are illustrated in Figure 8e,f. By stacking red and green PhC phosphor plates for sufficient fluorescence intensity, a WLED was built. It showed an 8% increase in the total emission intensity with the use of 33% less QD material compared to the reference device.<sup>[125]</sup> Recently, by applying the plasmonic color effect, Chen et al. demonstrated a metallodielectric wavelength selective reflector (WSR) based on Ag nanoparticles and a  $\text{TiO}_2$  coating layer. This WSR shows high transmittance in the UV and blue spectral regions as well as high reflectance in the green and red spectral ranges. A low-cost solid-state dewetting process was introduced to fabricate an Ag nanoparticle monolayer from a flat Ag thin film. The transmittance and reflectance spectra of the WSR can be altered by tailoring the size of Ag nanoparticles and the thickness of the  $\text{TiO}_2$  coating layer. As shown in Figure 8g,h, by in-

corporating the WSR into a QD-converted white LED, a radiant flux enhancement of 19.5% was obtained as the WSR can reflect the backward emission light from the QD film to the forward direction.<sup>[126]</sup>

While the abovementioned methods create an added surface structure layer on the QD composite, Chandrasekar and co-workers proposed a solvothermal method for producing nitrogen-rich carbon dots (CDs) and a self-assembled photonic-grade thin film of CD-doped PS material, which directly formed the QD composite into the desired microsphere structure. Owing to the efficient light-scattering capability of the microsphere structure (increasing the interaction time of the excitation light with the QD material), the photonic-grade composite composed of CD-doped PS microspheres exhibited a 22-fold enhancement in the photoluminescence intensity compared to the homogeneous PS-CD film.<sup>[127]</sup>

In summary, the internal doping structure is the most straightforward strategy; however, the enhancement is relatively low. The internal porous structure and surface structure strategies can achieve a more significant enhancement of the photoluminescence intensity. Still, phase separation and vapor deposition processes are relatively complex and expensive. Thus, an effective and cost-efficient method for improving the optical properties and stability of QD materials is required. Regarding the commercial application of mini/micro-LED displays, novel

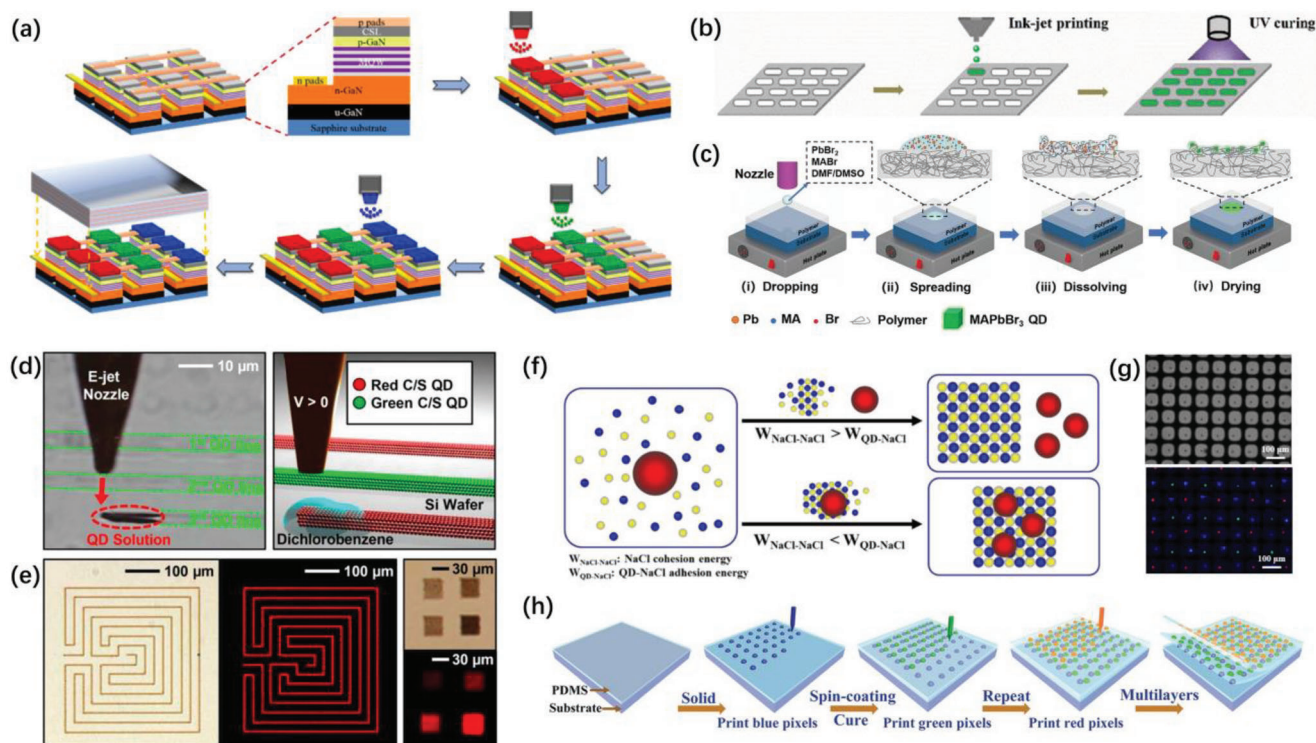


**Figure 9.** a) Process flow for a full-color emission QD-based micro-LED display via ink-jet printing. Reproduced with permission.<sup>[128]</sup> Copyright 2015, Optica Society. b) Schematic illustration of the PeQD color conversion film fabrication process by the ink-jet printing method using UV-curing ink. Reproduced with permission.<sup>[130]</sup> Copyright 2019, Wiley-VCH. c) Schematic diagram of the in situ ink-jet printing strategy for PeQDs. Reproduced with permission.<sup>[131]</sup> Copyright 2019, Wiley-VCH. d) Illustration of QD packaging in a salt crystal from an aqueous solution. e) Optical microscope images of salt-packaged QDs under visible light (left) and UV light (right). Reproduced with permission.<sup>[132]</sup> Copyright 2020, American Chemical Society. f) Microscopic image and schematic illustration of electrohydrodynamic jet printing. g) Optical (left) and fluorescence (right) images of QD pixels generated by electrohydrodynamic jet printing. Reproduced with permission.<sup>[133]</sup> Copyright 2015, American Chemical Society. h) Schematic illustration of layer-by-layer printed multicolor QD dot arrays. Reproduced with permission.<sup>[137]</sup> Copyright 2019, Wiley-VCH.

property-enhancing strategies for QDs that are adaptive to the existing display techniques and modules are the next key point in this field.

## 5. Fabrication and Applications of Pixelated QDs

The QD-enhanced mini/micro-LED display technology is enabled by a combination of the high efficiency of mini/micro-LEDs and superior optical properties of QD materials, which make it an excellent display solution with the best application prospects at present. Regarding the relatively low efficiency of green LED chips and the challenging mass transfer process of the RGB LED chip array, coating the QD color conversion medium on a blue mini/micro-LED chip seems to be the superior solution. In this case, the realization of pixelation of RGB QD materials is the next key issue for QD-based display technologies.

This section on the QD pixelation processes is divided into three subsections: printing, lithography, and transfer printing.

### 5.1. Printing Processes

Ink-jet printing (IJP) and aerosol-jet printing (AJP) are emerging and promising printing technologies. These two processes have

been demonstrated for printing a variety of electronic devices, including solar cells, LEDs, and sensors.

Kuo and co-workers proposed a backlight-free full-color LED display strategy by combining a UV micro-LED and AJP in 2015. As shown in **Figure 9a** with optimization of printing parameters, including the working distance, stage speed, and gas flow rate, they successfully sprayed RGB QDs on a micro-LED array with a spraying line width of 35  $\mu\text{m}$ . Finally, they obtained a display panel with a resolution of 282 pixels per inch in full color.<sup>[128]</sup> Subsequently, they fabricated a 35  $\mu\text{m} \times 35 \mu\text{m}$  rectangular well-array structure using a photolithography technique to confine the printed QDs to reduce the optical crosstalk effect and the coffee ring effect. Compared with the reference without a well-array structure, the crosstalk rate of the micro-LED panel decreased from 32.8% to nearly zero. To further improve the efficiency of UV conversion, a distributed Bragg reflector was applied to cover the surface of the micro-LED panel, which enhanced the blue, green, and red QD luminous intensities by 5%, 32%, and 23%, respectively.<sup>[129]</sup>

IJP technology has also been developed for PeQD materials. Duan et al. dispersed CsPbBr<sub>3</sub> PeQDs in a UV adhesive to prepare printable PeQD inks and obtained a PeQD color conversion layer using a mold-assistant IJP process. The fabrication process is illustrated in **Figure 9b**. As a result, a 6.6 in. active matrix PeQD

display prototype with a resolution of  $384 \times 300$  was produced in combination with a blue OLED backlight. The resulting device exhibited high stability: the light conversion efficiency only decreased by 1.4% after exposure to air and moisture for 30 d without additional protection.<sup>[130]</sup>

However, the mechanical dispersion of PeQDs in a polymer matrix is prone to aggregation and nonuniform dispersion, which can significantly degrade the optical performance of the color conversion layer. To address this problem, Zhong and co-workers proposed an in situ IJP method that directly printed a perovskite precursor solution onto polymeric substrates to fabricate PeQD pixels. The proposed method exhibited wide applicability for various PeQD materials and polymers, including polyacrylonitrile, PMMA, PS, polyvinyl chloride, polyvinylidene fluoride, cellulose acetate, and polyvinylidene chloride. In this method, as shown in Figure 9c, the precursors of the PeQDs were dissolved in DMF or dimethylsulfoxide solvents as ink and then printed on the heated polymer film to obtain the PeQD pixel after evaporation of the solvent. The accuracy of this IJP method can be adjusted by varying the printing temperature of the polymer substrate and nozzle size. PeQD patterns with a PLQY of up to 80% were obtained using this low-cost, large-area printing technique.<sup>[131]</sup>

Aiming at crystalline salt-packaged QD materials, Chen and co-workers compounded an MPA-modified hydrophilic QD material with a NaCl medium; then, using IJP, the deposited QDs were spontaneously packaged in a single NaCl crystal, as shown in Figure 9d,e. For incorporation with micro-LEDs, an RGB QD@NaCl array with small pixel size and uniform size distribution was fabricated by the IJP process, achieving an NTSC color gamut of  $\approx 110\%$ .<sup>[132]</sup>

Electrohydrodynamic printing (EHDP) requires a conductive nozzle and a conductive substrate as electrodes to generate an assisting electric field, which drives and controls the ink spray through the Coulomb force. In addition to the conventional printing parameters, EHDP allows extra electrical parameters, such as the voltage between electrodes and the waveform of the applied voltage, to be adjusted for better control of the printing process and more printing forms, including electro-spraying and electro-spinning.

The earliest report on combining the EHDP method with QD materials was published in 2015. Rogers and co-workers first optimized the material system and processing conditions for high-resolution printing of QDs, achieving precise control of the thickness and lateral resolution down to the sub-micrometer level using an electrohydrodynamic jet printing technique. In this process, as shown in Figure 9f,g, an electric field was applied between a metal-coated glass capillary as a printing nozzle and the conductive substrate to generate a controlled electrohydrodynamic jet of QD dichlorobenzene solution. The proposed method achieved a minimum line width of  $0.25 \mu\text{m}$  and enabled large-area printing.<sup>[133]</sup>

In 2017, Kuo and co-workers proposed that the emission wavelength of the device could be changed by lithographically defining a nanoscale ring array on a micro-LED chip, varying the thickness of the ring wall from 120 to 80 and 40 nm caused an emission shift from green to blue.<sup>[134]</sup> Based on this result, they developed

hybrid QD nanoring micro-LEDs (QD-NR- $\mu$ LEDs) for full-color displays using a super-IJP system (electrohydrodynamic printing) with a printing line width of  $1.65 \mu\text{m}$  to prepare a QD color conversion layer with high precision. In this fabrication method, a green LED chip with an emission wavelength of 525 nm was utilized and divided into three subpixel regions of  $3 \mu\text{m} \times 10 \mu\text{m}$  for the RGB color. The green region was left untreated, and a nanoring structure was fabricated by photolithography in the other two regions to shift the emission to blue light. Then they printed red QDs in the red area and finally incorporated a Bragg reflector to complete the manufacturing of the full-color micro-LED. The obtained device achieved a nonradiative resonant energy transfer efficiency of 66.4% and high color gamut performance of 104.8% NTSC and 78.2% Rec. 2020.<sup>[135]</sup>

To reduce the coffee rings that deteriorate the quality of the printed QD color conversion layer, Yin and co-workers investigated and optimized the QD ink used for EHDP with mixed solvents of cyclohexylbenzene and nonane. With an optimal volume ratio of cyclohexylbenzene to nonane of 8:2, the printed QD layers exhibited high quality, high resolution, and nice film morphology.<sup>[136]</sup> Li and co-workers developed a high-precision layer-by-layer printing technique without a mold and prepared high-resolution scalable and full-color flexible QD layers. Based on EHDP, they printed QD ink on PDMS. Subsequently, another layer of PDMS was spin-coated to achieve layer-by-layer printing without any patterned substrate or mask, as shown in Figure 9h. By controlling the pre-curing time of the PDMS and the pulse voltage, the printing resolution could be varied from 0.89 to  $12.3 \mu\text{m}$ . Due to the layered structure, the interaction between the materials could be reduced, resulting in good color stability. This method integrates high-resolution multicolor pixels directly onto a flexible substrate to produce a pixelated full-color light-emitting layer, which has great potential for nanopatterned applications of flexible wearable optoelectronic devices.<sup>[137]</sup>

Compared to other printing techniques, the EHDP process can achieve a higher resolution and better control. However, EHDP requires a conductive substrate to generate the necessary electric field. This limits the applicability of this method. Moreover, applying an electric field to drive the formation of the material also causes a side effect on the ink itself, especially for materials such as carbon nanotubes and graphene, which are electrically conductive.

Overall, printing in general is highly process-controllable, flexible, mask-free, and material-compatible, and it is also very efficient in terms of material utilization. However, its accuracy is strongly dependent on the printing equipment, especially the performance of the nozzle and the properties of the ink. The solidification of the ink after printing is accompanied by complex hydro- and thermodynamic processes. This can easily cause morphological defects, such as the agglomeration of QD inks and the coffee ring effect. Both reduce the overall optical performance and efficiency of the device. The organic solvents commonly used in the printing process cause problems such as environmental pollution and toxicity to humans. For large-scale industrial applications, there is a need to improve the production efficiency and capacity of the printing process. These issues need to be addressed and are important topics for future research on this technology.

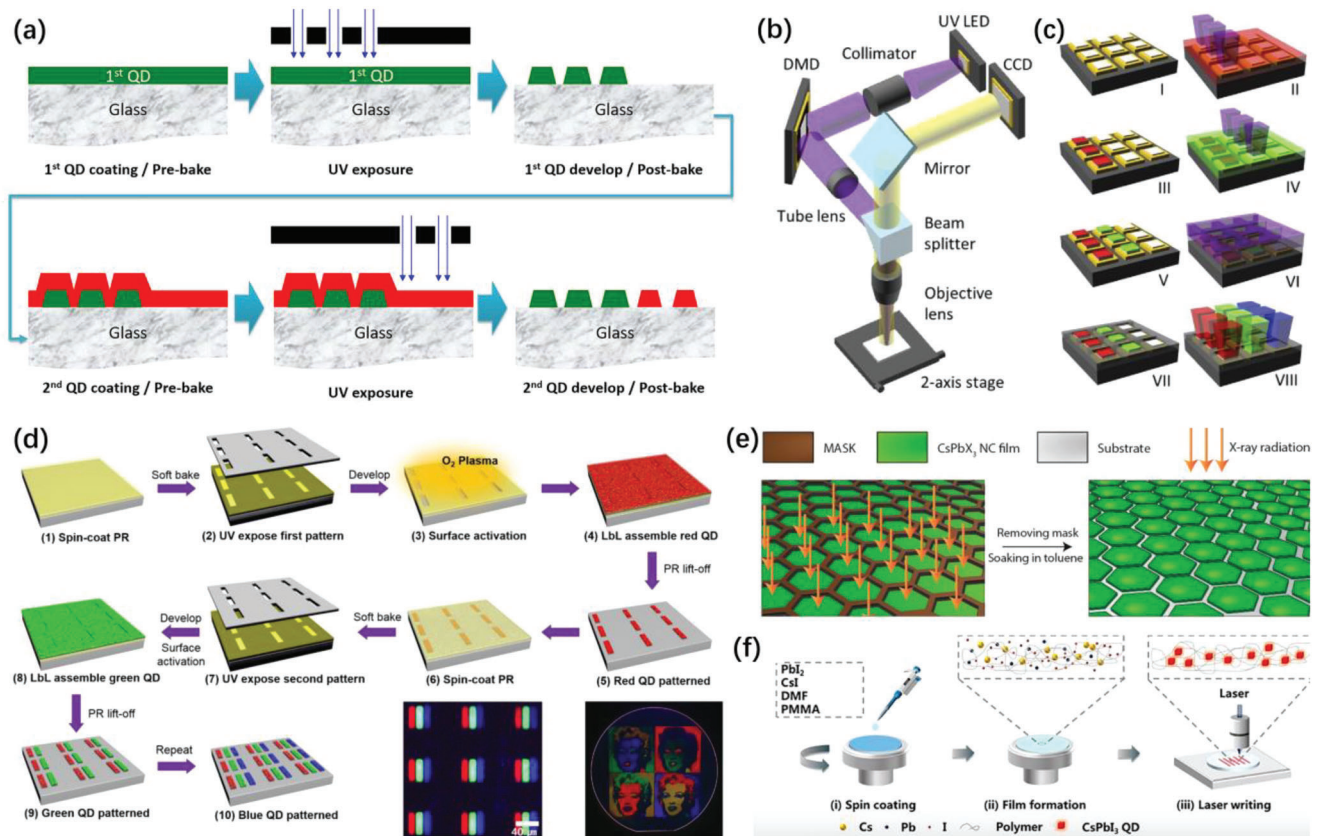


**Figure 10.** a) Process flow to form green and red QD color conversion layers on the same plane by direct photolithography. Reproduced with permission.<sup>[138]</sup> Copyright 2019, Society for Information Display. b) Schematic of the UV-based digital light processing projection lithography system. Reproduced with permission.<sup>[139]</sup> Copyright 2019, Optica Society. c) Schematic of the pixelation procedure for red and green color converters on a blue micro-LED array for an RGB full-color display using digital light processing lithography. Reproduced with permission.<sup>[141]</sup> Copyright 2016, American Chemical Society. d) Schematic of pixelating different QDs on a substrate using repeated photolithography and layer-by-layer assembly and the fabricated patterns under UV excitation. Reproduced with permission.<sup>[141]</sup> Copyright 2016, American Chemical Society. e) Schematic representation of X-ray lithography for PeQD film pixelation. Reproduced with permission.<sup>[144]</sup> Copyright 2016, The Authors, published by American Chemical Society. f) In situ direct laser-writing fabrication of pixelated  $\gamma$ -CsPbI<sub>3</sub> PeQDs. Reproduced with permission.<sup>[146]</sup> Copyright 2021, American Chemical Society.

## 5.2. Lithography-Based Processes

Lithography-based processes are widely utilized for nano/microstructure formation. Among them, the photolithography process is the most common method owing to its advantages of low cost, large scale, and relatively low equipment requirements in the case of optoelectronic devices. Regarding QD materials, photolithography has been introduced for the pixelation of QD color conversion layers in many studies. In this section, we review these studies, dividing them into two main categories: direct photolithography and indirect photolithography methods. Direct photolithography is defined as the direct mixing of QD materials with a photosensitive matrix, followed by pixelation of the QD/photoresist composite using a conventional photolithography process. Indirect photolithography refers to the fabrication of a patterned mold by a photolithography process, followed by further patterning of the QD material based on this textured mold using specific additional steps. A UV light source is used to fabricate nano-/micropixels in the photoresist with a mask. Moreover, various lithography methods, such as laser and X-ray lithography, have been investigated and developed

for the structural formation of QD materials; these studies are categorized as other lithography processes in this review.

### 5.2.1. Direct Photolithography

Based on the mechanical dispersion method, in 2019, Jang and co-workers proposed a photopatternable QD photoresist by mixing the QD solution, resin, curing agent, additives, and photoinitiator into propylene glycol monomethyl ether acetate solvent. After carrying out the sequential photolithography processes, a full-color QD color conversion layer with a high pixel resolution was fabricated for a micro-LED display. The fabrication process for the QD color conversion layer is shown in **Figure 10a**. By optimizing the recipe for the QD photoresist, pixelated QD patterns with a size of  $10\ \mu\text{m} \times 10\ \mu\text{m}$  and a minimum thickness of  $12\ \mu\text{m}$  were obtained.<sup>[138]</sup>

In the same year, Fang and co-workers developed a mask-free projection lithography method using a UV digital light processing printer for direct photolithography on a QD color conversion layer, schematically shown in **Figure 10b,c**. The most critical part

of this system is a digital micromirror device (DMD), which can be flipped by a digital signal at a high frequency. The UV beam is dynamically reflected by the aluminum layer of the DMD, focused by the objective lens, and finally projected onto the QD layer for micropatterning. Consequently, a minimum pixel size of 6  $\mu\text{m}$  was achieved. Moreover, as the incompatibility between QD materials and photoresists leads to the degradation of QD performance, a thiol–ene photopolymer matrix was chosen for better dispersion of the amine surface group capped QDs. Concentrations of even up to 100  $\text{mg mL}^{-1}$  could be achieved. As a result, a conversion efficiency enhancement by 50–100% compared to the drop-casted QD layer was achieved.<sup>[139]</sup>

In 2020, Bae and co-workers proposed a pixelated color filter containing high concentrations of red (10 wt%) and green (20 wt%) QDs in a siloxane matrix based on a photolithography method. A ligand-exchange treatment was first performed to transfer the oleic acid-capped QDs to mercapto-silane-capped QDs (MS-QDs), followed by a non-hydrolytic sol–gel condensation to synthesize the MS-QD-dispersed methacrylate oligosiloxane resin. With the improved ligand system, the QDs exhibited excellent dispersibility in the siloxane matrix and superior stability under harsh heat and moisture conditions (85 °C/5% RH and 85 °C/85% RH), and exposure to chemicals (EtOH, HCl, and NaOH) compared with conventional QD/resist composites. By incorporating the color filter with a blue LED chip, a wide NTSC color gamut of 108% was achieved.<sup>[140]</sup>

### 5.2.2. Indirect Photolithography

In addition to the direct photolithography of QD/resist composites, indirect pixelation methods based on photolithography processes have been widely investigated. Han and co-workers proposed a charge-assisted layer-by-layer assembly technique in combination with conventional photolithography to form multicolor microscale QD pixels in large areas. A schematic of the fabrication process is shown in Figure 10d. This method used a Si wafer coated with a 1- $\mu\text{m}$ -thick  $\text{SiO}_2$  layer as the substrate. A conventional photolithography process was performed to fabricate a patterned photoresist on the substrate, followed by oxygen plasma exposure to attach a negative charge to the uncovered areas of the substrate. The substrate was subsequently immersed in a PDDA solution to obtain a positively charged surface in these areas. Water-soluble QDs were adhered to the surface by simply covering the substrate with an aqueous QD solution. By repeating the above assembly process, multicolor QD materials could be pixelated layer-by-layer on the substrate. Eventually, a full-color pixelated QD film with a pixel size of 40  $\mu\text{m} \times 40 \mu\text{m}$  was fabricated, enabling the high-resolution RGB display and achieving a maximum electroluminescence intensity of 23 770  $\text{cd m}^{-2}$ .<sup>[141]</sup>

Ju and co-workers demonstrated an efficient multilayer pixelation method for full-color QD displays utilizing spatial light-assisted and locally controlled surface tailoring via photochemical deactivation. In this study, PEI, a strong interconnecting polymer, was chosen for spatial light patterning because of its high density of amine functional groups which allow it to be employed as both a charge transfer and anchor material for QD materials and inorganic surfaces. Moreover, the photolytic decomposition of PEI and its amine groups leads to the loss of its functionali-

ties, enabling locally controlled surface tailoring of the PEI layer when incorporated with a lithography mask. A PEI layer was first spin-coated on a glass substrate, followed by UV exposure with a quartz mask to decompose the PEI layer in the areas where the QDs should not be deposited. Then, the QD solution was spin-coated and annealed on the PEI layer, followed by a rinsing process with toluene. A full-color pixelated QD layer was obtained by repeating the above procedure three times.<sup>[142]</sup>

### 5.2.3. Other Lithography Processes

In addition to the classical photolithography process, various direct-writing lithography methods and unconventional light sources have been introduced for the pixelation of QD materials. Thourhout and co-workers utilized electron-beam lithography to fabricate structured photoresists and then deposited single-layer QDs using Langmuir–Blodgett deposition and a subsequent optimized peeling process. The fabricated QD pixels could realize feature sizes as small as 30 nm with the desired shape and demonstrated the formation of single-QD patterns with a single-QD deposition yield of up to 40%.<sup>[143]</sup>

Manna and co-workers introduced an X-ray lithography process for fabricating pixelated PeQD layers. Figure 10e shows that a  $\text{CsPbX}_3$  ( $X = \text{I, Br, or Cl}$ ) PeQD thin film was first deposited on a silicon substrate by solution drop-casting or spin-coating, followed by selective irradiation with low-flux X-rays from an X-ray photoelectron spectrometer source in the presence of a mask. The organic ligands capping the surface of the PeQDs form intermolecular C=C bonds under X-ray irradiation. This introduces additional properties to the X-ray-exposed region of the PeQD film, including insolubility in organic solvents and better resistance to air and moisture. Therefore, a pixelated PeQD film can be prepared after further rinsing with organic solvents without an additional photoresist, exhibiting excellent stability and an extended lifetime.<sup>[144]</sup>

The direct laser writing technique has also been widely investigated. Sun and co-workers applied femtosecond direct laser writing to achieve a programmable assembly of CdTe QD layers. Driven by the focused femtosecond laser beam, arbitrarily shaped photocrosslinked pixels with a resolution reaching 170 nm were achieved for the QD layer. This opens up a new alternative for the flexible fabrication and pixelation of QD materials. Moreover, owing to the ultrafast femtosecond laser pulses, the thermal energy generated during lithography was negligible, which could effectively suppress the thermally induced performance quenching of QD materials.<sup>[145]</sup> Based on the difference in thermal conductivity between the polymer matrix and PeQDs, Zhong et al. targeted structured PeQD materials by utilizing a 405 nm nanosecond laser as the light source to perform DLW on a polymer film containing the precursors of  $\gamma\text{-CsPbI}_3$  PeQDs, as shown in Figure 10f. A fluorescent PeQD grating with a period of 4  $\mu\text{m}$  and a PLQY of up to 92% was obtained. By varying the power and scanning speed, the line width of the pixelated  $\gamma\text{-CsPbI}_3$  PeQDs could be adjusted, and the minimum line width could be reduced to 900 nm.<sup>[146]</sup> In addition, Zeng et al. performed a direct laser writing process on a spin-coated PeQD thin film without a polymer matrix. Similar to the X-ray lithography method, the laser exposure could remove surface ligands such as oleic acid or oleyl

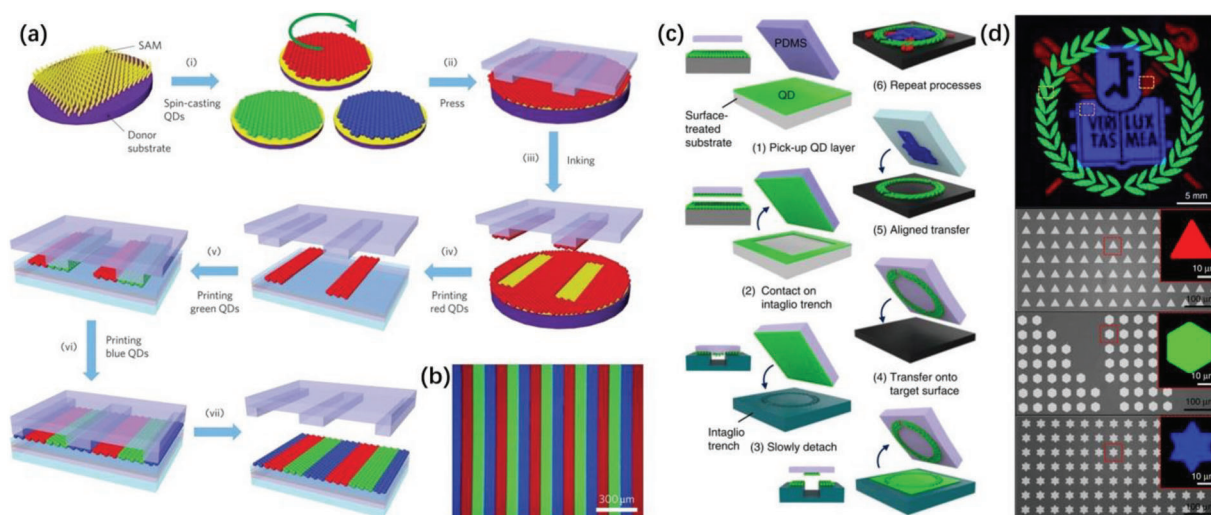


**Figure 11.** a) Schematic of the transfer-printing process for pixelation of quantum dots. b) Fluorescence micrograph of transfer-printed RGB QD stripes on a glass substrate, excited by 365 nm UV radiation. Reproduced with permission.<sup>[149]</sup> Copyright 2011, Springer Nature Limited. c) Schematic illustration of the intaglio transfer-printing process (the inset images on the left of each frame show the side view). d) Photoluminescence image magnified views of the RGB QD pixels produced via multiple aligned transfer printing. Reproduced with permission.<sup>[150]</sup> Copyright 2015, The Authors, under the Creative Commons CC BY license.

amine from the PeQDs, resulting in the insolubility of the irradiated area in organic solvents. Therefore, the desired patterns were obtained using a solvent rinsing process after the laser writing. This laser-writing lithography method exhibited high flexibility as a mask-free process with lower equipment requirements because it utilized a UV laser as the excitation source, which enables its application in large-scale fabrication.<sup>[147]</sup>

### 5.3. Transfer Printing Process

Transfer printing describes a group of processes that assemble the desired material on a prestructured surface or into a spatially organized shape and then transfer the patterned layer of the material to the final substrate. This method can be utilized in the fabrication of the black matrix for QDs as well.<sup>[148]</sup> For QD pixelation, designing effective assembly and transfer strategies based on the difference in affinity of the master and substrate for QD materials is the key to this process.

Classically, Kim et al. demonstrated a full-color, large-scale QD printing technique for displays using a transfer printing process in a relief printing form. A flowchart of the process is shown in **Figure 11a,b**. A uniform QD layer was spin-coated on a substrate with low surface energy. The substrate's surface was modified by an octadecyltrichlorosilane solution to enable delamination at the interface. As the surface energy of PDMS is slightly lower than that of the modified substrate, the QD layer is partly picked up and transferred by the protruding stripes of the textured PDMS stamp and subsequently brought into contact with a receiving substrate to realize the stacking of full-color QD microstrips. This solvent-free transfer printing process can be used to create large-scale QD-based optoelectronic devices with well-ordered micropatterns.<sup>[149]</sup>

Based on another printing form, Hyeon and co-workers proposed an intaglio transfer printing technology for fabricating

RGB QD pixels with a resolution of up to 2460 pixels per inch. As shown in **Figure 11c,d**, the QD material was first spin-coated onto a pretreated silicon substrate, and then a planar PDMS stamp was utilized for fast pickup ( $10 \text{ cm s}^{-1}$ ) of the QD layer. The QD layer was transferred and further contacted on a structured intaglio trench at low pressure and slowly detached to obtain the residual patterned QD layer on the PDMS stamp. Consequently, the QD pattern was transferred to the target substrate. A full-color pixelated QD layer was obtained by repeating the transfer-printing process. Based on a comparison, the printing accuracy and transfer yield of the intaglio transfer printing process was better than those of the relief printing form.<sup>[150]</sup>

The main advantages of the transfer printing technology are its capabilities for large-scale pixelation and the dry transfer of QD materials, which can reduce the crosstalk of pixels. However, this technology requires a prestructured master for a specific desired pattern. This reduces the flexibility of the process and diminishes the forming accuracy after repeated use of the master, limiting its application prospects.

In the practical applications of full-color display, various scales of pixel sizes are demanded for different types of devices. For example, the mesa size of large-panel displays is typically larger than  $20 \mu\text{m}$ , while the subpixel size for AR devices is only  $\approx 2 \mu\text{m}$ . The selection of the pixelation method should be based on a comprehensive consideration including the goal pixel size, the production efficiency and cost of the process, and the compatibility with the QD materials. For better comparison, we summarize the characteristics of the pixelation methods mentioned in **Table 2**. In general, as mask-free processes, IJP and AJP methods have high usage rates and nice compatibility with material that are cost-efficient for mass production. However, the pixel size they can achieve is normally larger than  $10 \mu\text{m}$ , which is not sufficient for AR/VR applications. EHDP methods can significantly reduce the feature size of the printing process to even lower than  $1 \mu\text{m}$ . The drawback is that the additional electric field is

**Table 2.** Characteristics of the pixelation methods for QDs.

Method	Feature size	QD material	Color of emission	Refs.
Aerosol jet printing	30 $\mu\text{m}$ (line width)	CdS, CdSe/ZnS	RGB	[128]
Inkjet printing	200 $\mu\text{m}$ $\times$ 75 $\mu\text{m}$ (pixel size)	CsPbBr <sub>3</sub>	Green	[130]
Inkjet printing	110 $\mu\text{m}$ (pixel size)	MAPbBr <sub>3</sub>	Green	[131]
Electrohydrodynamic printing	3.9 $\mu\text{m}$ (dot size) $\approx$ 400 nm (line width)	CdSe/CdZnSeS, CdSe/CdS/ZnS	Red, green	[133]
Electrohydrodynamic printing	1 $\mu\text{m}$ (dot size)	CdSe/CdS/ZnS	Red	[136]
Electrohydrodynamic printing	$\approx$ 890 nm (line width)	CdSe	RGB	[137]
Photolithography	10 $\mu\text{m}$ (pixel size)	–	Red, green	[138]
Projection lithography	21 $\mu\text{m}$ (pixel size)	CdSe/ZnS	Red, green	[139]
Indirect photolithography	5 $\mu\text{m}$ (line width)	II–VI core–shell QDs	RGB	[141]
Indirect photolithography	8 $\mu\text{m}$ $\times$ 40 $\mu\text{m}$ (pixel size)	CdSe/ZnS	RGB	[142]
E-beam lithography	$\approx$ 30 nm (line width)	CdSe/CdS	Red	[143]
X-ray lithography	150 $\mu\text{m}$ (pixel size)	CsPbI <sub>3</sub> , CsPbBr <sub>3</sub>	Red, green	[144]
Laser direct writing	$\approx$ 170 nm (line width)	CdTe	Green	[145]
Laser direct writing	900 nm (line width)	CsPbI <sub>3</sub>	Red	[146]
Laser direct writing	3.3 $\mu\text{m}$ (line width)	CsPbBr <sub>3</sub>	Red	[147]
Transfer printing	400 nm (line width)	CdSe/CdS/ZnS, CdSeS, CdS	RGB	[149]
Transfer printing	6 $\mu\text{m}$ (pixel size)	CdSe/ZnS, CuInSe, PbS	RGB	[150]

incompatible with some of the QD materials (e.g., conductive carbon-based QD). Direct photolithography methods are only capable of pixelating QDs in a photoresist matrix, which limits the prospect of applications. To avoid this problem, indirect lithography methods pixelate the QDs based on the prepatterned structure and demonstrate a decent feature size below 10  $\mu\text{m}$ . Nevertheless, the processes of these methods are rather complex and increase the manufacturing costs. The high cost and relatively low production efficiency is an obstacle for e-beam lithography as well. Despite the impressive resolution for patterning QDs, the low processing speed of the method diminishes the potential for large-scale fabrication. Laser direct writing methods are promising for QD pixelation due to the ultrafine feature size. By manipulating the power and spot size of the laser, a nice balance between patterning resolution and processing speed can potentially be achieved for mass production. Transfer printing methods are also feasible for the large-scale fabrication of QD pixels with high resolution. However, the transfer process is based on the surface contact between the printing master and QDs which results in a low thickness of the QD layer. Thus, this patterning strategy is more suitable for preparing electroluminescent QD LEDs than fabricating a QD color conversion layer that requires higher thickness for light absorption.

#### 5.4. Applications of QDs in Mini/Micro-LED Display

To practically manufacture a QD-integrated mini/micro-LED device, complex works including fabrication of micro-LED chip array, building well-run bonding with the active driving matrix, and pixelating QD layer, are inevitable and make research highly challenging. In 2015, Kuo and co-workers utilized aerosol jet printing for depositing RGB QDs on top of a UV LED chip array, building a prototype of a full-color display device based on micro-

LED and QD color conversion. Owing to the excellent color purity of QDs, the panel showed a broad color gamut covering 1.52 times of the area of the NTSC color gamut.<sup>[128]</sup> Later on, they introduced nanoring structures to the surface of green LED epitaxial layer to tune the emission from green to blue through strain relaxation caused by the nanoring structure. Red QDs were subsequently deposited on the miniature LED chips with a pixel size of 3  $\mu\text{m}$   $\times$  10  $\mu\text{m}$  via super inkjet printing system for generating three primary colors. With incorporating distributed Bragg mirrors, a wide color gamut that overlapped 104.8% of NTSC color space and 78.2% of Rec. 2020 was obtained by the device.<sup>[129]</sup> Aiming at high-performance near-eye displays, Lee and co-workers integrated multiple fabrication technologies for producing a GaN-based micro-LED array with well-patterned QD micropixels, achieving a full-color display based on QD color conversion. In the fabrication, an epilayer transfer method comprising an alloy layer was designed for improved patterning the GaN semiconductor layer. Moreover, a repeated photolithography process was utilized for the pixelation of red and green QD layers. As a result, a high-resolution of 1270 PPI exceeding the retinal limit was achieved. With the thickness optimization of the QD layers, devices integrated with green QDs obtained an EQE over 36% while that of the device with red QDs was over 38%.<sup>[151]</sup> By adopting repeated photolithography in the fabrication, Jang and co-workers demonstrated a well patterned QD color conversion layer with a feature size down to 10  $\mu\text{m}$ . The green and red color conversion layers were then integrated with the active matrix of micro-LEDs to achieve a full-color display.<sup>[138]</sup> In addition, Hsiang et al. demonstrated a color-converted micro-LED display device with a micropatterned cholesteric liquid crystal (CLC) film as a self-assembly Bragg reflector for enhancing PL intensity. The feature size of the CLC film could be adjusted from 10 to 80  $\mu\text{m}$  via a patterned UV curing process. The integration of the CLC layer doubled the optical efficiency of the micro-LED display

device while maintaining the color gamut of  $\approx 90\%$  Rec. 2020.<sup>[152]</sup> By now, there the amount of work that addresses the complete fabrication process of QD-converted mini/micro-LED panel is still limited. Comprehensive investigations of optimizing the whole displaying system based on QDs and mini/micro-LED display are needed.

Besides, promising mini/micro-LED devices and panels have been continually launched by industry in recent years. In 2022, PlayNitride introduced a 0.49-in. color-converted micro-LED panel with a resolution of 4536 PPI (1920 × 1080).<sup>[153]</sup> In 2023, JBD exhibited a 0.13-in. monochrome micro-LED panel with an impressive pixel density of 6350 PPI and integrated with an RGB color projector through an X-cube for near-eye displays.<sup>[154]</sup> The launch of high-performance mini/micro-LED products effectively promotes this display technology to a broader market.

## 6. Summary

The introduction of QD materials presents an effective technical route to realize the full-color functionality of the mini/micro-LED-based display technology. We reviewed studies on QD materials and their application to mini/micro-LED displays. Four aspects of the research were discussed: the photoluminescence properties of QD materials, solid-state packaging of QDs in composites, light management of QD composites, and fabrication and applications of pixelated QD films.

As Cd-based QD materials can cause severe environmental damage and toxicity, In-based QDs can be potentially applied as Cd-free alternatives with further improvement in their photoluminescence performance attracting considerable attention and interest.

QD materials must be packaged in a solid-state matrix for subsequent processing and applications to achieve better stability and processability. The mechanical dispersion method and in situ polymerization method are relatively simple and the most commonly used methods. They are, however, highly dependent on utilizing organic solvents that are harmful, limiting their application prospects. The surface modification method is based on surface functional groups of QD materials and chemical modifications to improve the adaption of QDs to the packaging material. These methods, however, have demanding challenges for the chemical control of the interactions.

After packaging, the QD composites can be further enhanced in terms of optical performance and stability by various methods before being integrated into devices. The adsorbing-doping method utilizes an extra adsorber, such as mesoporous silica, for better packaging and light extraction compared with the direct doping of scattering particles. Strategies based on internal porous and surface structures exhibit a pronounced effect on increasing the luminescence intensity of QDs, but these processes are more complex and demanding. Such methods for the light management of the QD layer need to be adaptive to the pixelation process for pixel fabrication. This is a further obstacle that needs to be solved in this field.

The main processes for QD pixelation can be categorized into three types: direct printing, lithography, and transfer printing. The direct printing process has advantages in that it is noncontact, mask-free, and has good compatibility with QD solutions. Nevertheless, the formation accuracy is highly dependent on the

properties of the ink, and the production efficiency is relatively low. The lithography process can achieve high-resolution and large-scale fabrication, but the photoresist material limits its feasibility. The transfer printing process can directly operate with a dry QD layer without an organic solvent during the pixelation process, which generates less toxicity and can prevent cross-contamination between pixels. However, the approach is not yet sufficiently flexible, as it requires a printing template for the pattern and cannot achieve high resolutions.

Developing a more efficient and high-resolution pixelating process for QD materials remains an important research direction. A system that includes material synthesis, packaging, and pixelation needs to be further developed and optimized to promote the industrialization of QD-based mini/micro-LED display technologies.

## Acknowledgements

The authors gratefully acknowledge support from the Karlsruhe School of Optics and Photonics and the China Scholarship Council. This research was also funded by the Deutsche Forschungsgemeinschaft (DFG, German Research Foundation) under Germany's Excellence Strategy via the Excellence Cluster 3D Matter Made to Order (EXC-2082/1-390761711) and through the DFG priority program SPP 1839 "Tailored disorder".

Open access funding enabled and organized by Projekt DEAL.

## Conflict of Interest

The authors declare no conflict of interest.

## Keywords

color conversion, display technology, microstructure, mini/microlight-emitting diodes, quantum dots

Received: April 13, 2023

Revised: July 13, 2023

Published online:

- [1] V. W. Lee, N. Twu, I. Kyriassis, *Inf. Disp.* **2016**, 32, 16.
- [2] H. Chen, J. He, S.-T. Wu, *IEEE J. Sel. Top. Quantum Electron.* **2017**, 23, 1900611.
- [3] S. X. Jin, J. Li, J. Z. Li, J. Y. Lin, H. X. Jiang, *Appl. Phys. Lett.* **2000**, 76, 631.
- [4] R. H. Horng, H. Y. Chien, F. G. Tarntair, D. S. Wu, *IEEE J. Electron Devices Soc.* **2018**, 6, 1064.
- [5] Y. Huang, E. L. Hsiang, M. Y. Deng, S. T. Wu, *Light: Sci. Appl.* **2020**, 9, 105.
- [6] A. Paranjpe, J. Montgomery, S. M. Lee, C. Morath, *Dig. Tech. Pap. - Soc. Inf. Disp. Int. Symp.* **2018**, 49, 597.
- [7] J. Xiong, E.-L. Hsiang, Z. He, T. Zhan, S.-T. Wu, *Light: Sci. Appl.* **2021**, 10, 216.
- [8] E.-L. Hsiang, Z. Yang, Q. Yang, P.-C. Lai, C.-L. Lin, S.-T. Wu, *Adv. Opt. Photonics* **2022**, 14, 783.
- [9] "Global Micro-LED Market with Covid-19 Impact Analysis by Application (Display (Smartwatch, NTE Device, Smartphone and Tablet, Television, Digital Signage), Lighting (General, Automotive)), Display Panel Size, Vertical

- and Region – Forecast to 2027”, Research and Markets, <https://www.researchandmarkets.com/reports/5067415/global-micro-led-market-with-covid-19-impact> (accessed: December 2021).
- [10] T. Wu, C. W. Sher, Y. Lin, C. F. Lee, S. Liang, Y. Lu, S. W. H. Chen, W. Guo, H. C. Kuo, Z. Chen, *Appl. Sci.* **2018**, *8*, 1557.
- [11] R. S. Cok, M. Meitl, R. Rotzoll, G. Melnik, A. Fecioru, A. J. Trindade, B. Raymond, S. Bonafede, D. Gomez, T. Moore, C. Prevatte, E. Radauscher, S. Goodwin, P. Hines, C. A. Bower, *J. Soc. Inf. Disp.* **2017**, *25*, 589.
- [12] B. Corbett, R. Loi, W. Zhou, D. Liu, Z. Ma, *Prog. Quantum Electron.* **2017**, *52*, 1.
- [13] J. T. Oh, S. Y. Lee, Y. T. Moon, J. H. Moon, S. Park, K. Y. Hong, K. Y. Song, C. Oh, J. I. Shim, H. H. Jeong, J. O. Song, H. Amano, T. Y. Seong, *Opt. Express* **2018**, *26*, 11194.
- [14] P. Royo, R. P. Stanley, M. Ilegems, K. Streubel, K. H. Gulden, *J. Appl. Phys.* **2002**, *91*, 2563.
- [15] J. J. Wierer, N. Tansu, *Laser Photonics Rev.* **2019**, *13*, 1900141.
- [16] K. A. Bulashevich, S. Y. Karpov, *Phys. Status Solidi RRL* **2016**, *10*, 480.
- [17] C. Yan, G. Liang, G. Liu, Y. Tang, J. Li, Z. T. Li, *IEEE Trans. Electron Devices* **2021**, *68*, 584.
- [18] Y. Liu, J. Silver, R. J. Xie, J. Zhang, H. Xu, H. Shao, J. Jiang, H. Jiang, *J. Mater. Chem. C* **2017**, *5*, 12365.
- [19] Y. H. Kim, N. S. M. Viswanath, S. Unithrattil, H. J. Kim, W. B. Im, *ECSS J. Solid State Sci. Technol.* **2017**, *7*, R3134.
- [20] Z. T. Li, C. J. Song, Q. L. Zhao, J. S. Li, J. L. Zheng, Y. Tang, *IEEE Trans. Compon., Packag., Manuf. Technol.* **2020**, *10*, 1204.
- [21] X. Bai, H. Yang, B. Zhao, X. Zhang, X. Li, B. Xu, F. Wei, Z. Liu, K. Wang, X. W. Sun, *Dig. Tech. Pap. - Soc. Inf. Disp. Int. Symp.* **2019**, *50*, 30.
- [22] Y. E. Panfil, M. Oded, U. Banin, *Angew. Chem., Int. Ed.* **2018**, *57*, 4274.
- [23] F. P. García de Arquer, D. V. Talapin, V. I. Klimov, Y. Arakawa, M. Bayer, E. H. Sargent, *Science* **2021**, *373*, 8541.
- [24] F. Wei, S. Li, X. Bai, Z. Liu, *Dig. Tech. Pap. - Soc. Inf. Disp. Int. Symp.* **2018**, *49*, 697.
- [25] J. H. Kang, J. Han, *Dig. Tech. Pap. - Soc. Inf. Disp. Int. Symp.* **2019**, *50*, 914.
- [26] Z. Li, J. Zheng, J. Li, W. Zhan, Y. Tang, *Opt. Express* **2020**, *28*, 13279.
- [27] M. Diaz-Gonzalez, A. de la Escosura-Muniz, M. T. FernandezArguelles, F. J. G. Alonso, J. M. Costa-Fernandez, *Surface-Modified Nanobiomaterials for Electrochemical and Biomedicine Applications*, Springer. Cham **2020**, p. 133.
- [28] Z. T. Li, H. W. Zhang, J. S. Li, K. Cao, Z. Chen, L. Xu, X. R. Ding, B. H. Yu, Y. Tang, J. Z. Ou, H. C. Kuo, H. L. Yip, *Adv. Sci.* **2022**, *9*, 2201844.
- [29] S. Mei, X. Liu, W. Zhang, R. Liu, L. Zheng, R. Guo, P. Tian, *ACS Appl. Mater. Interfaces* **2018**, *10*, 5641.
- [30] N. Ming, S. Tao, W. Yang, Q. Chen, R. Sun, C. Wang, S. Wang, B. Man, H. Zhang, *Opt. Mater. Express* **2018**, *26*, 9017.
- [31] J. Li, Y. Tang, Z. Li, X. Ding, D. Yuan, B. Yu, *Materials* **2017**, *10*, 1264.
- [32] J. S. Li, Y. Tang, Z. T. Li, X. R. Ding, L. S. Rao, B. H. Yu, *IEEE Trans. Electron Devices* **2018**, *65*, 2877.
- [33] J. S. Li, Y. Tang, Z. T. Li, K. Cao, C. M. Yan, X. R. Ding, *Nanotechnology* **2018**, *29*, 295707.
- [34] A. I. Ekimov, A. A. Onushchenko, *JETP Lett* **1981**, *34*, 363.
- [35] K. Kalyanasundaram, E. Borgarello, D. Duonghong, M. Grätzel, *Angew. Chem., Int. Ed.* **1981**, *20*, 987.
- [36] R. Rossetti, S. Nakahara, L. E. Brus, *J. Chem. Phys.* **1983**, *79*, 1086.
- [37] T. Takagahara, *Phys. Rev. B* **1987**, *36*, 9293.
- [38] W. Que, G. Kirzzenow, *Phys. Rev. B* **1988**, *38*, 3614.
- [39] N. Peyghambarian, B. Fluegel, D. Hulin, A. Migus, M. Joffre, A. Antonetti, S. W. Koch, M. Lindberg, *IEEE J. Quantum Electron.* **1989**, *25*, 2516.
- [40] V. L. Colvin, M. C. Schlamp, A. P. Alivisatos, *Nature* **1994**, *370*, 354.
- [41] D. V. Talapin, J. S. Lee, M. V. Kovalenko, E. V. Shevchenko, *Chem. Rev.* **2010**, *110*, 389.
- [42] M. A. Hines, P. Guyot-Sionnest, *J. Phys. Chem.* **1996**, *100*, 468.
- [43] D. A. Hanifi, N. D. Bronstein, B. A. Koscher, Z. Nett, J. K. Swabeck, K. Takano, A. M. Schwartzberg, L. Maserati, K. Vandewal, Y. van de Burgt, A. Salleo, A. P. Alivisatos, *Science* **2019**, *363*, 1199.
- [44] J. Hao, H. Liu, J. Miao, R. Lu, Z. Zhou, B. Zhao, B. Xie, J. Cheng, K. Wang, M. H. Delville, *Sci. Rep.* **2019**, *9*, 12048.
- [45] X. Jin, K. Xie, T. Zhang, H. Lian, Z. Zhang, B. Xu, D. Li, Q. Li, *Chem. Commun.* **2020**, *56*, 6130.
- [46] B. Xu, T. Zhang, X. Lin, H. Yang, X. Jin, Z. Huang, Z. Zhang, D. Li, Q. Li, *Opt. Mater. Express* **2020**, *10*, 1232.
- [47] K. Kim, Y. H. Suh, D. Kim, Y. Choi, E. Bang, B. H. Kim, J. Park, *Chem. Mater.* **2020**, *32*, 2795.
- [48] Y.-H. Won, O. Cho, T. Kim, D.-Y. Chung, T. Kim, H. Chung, H. Jang, J. Lee, D. Kim, E. Jang, *Nature* **2019**, *575*, 634.
- [49] F. Huang, C. Bi, R. Guo, C. Zheng, J. Ning, J. Tian, *J. Phys. Chem. Lett.* **2019**, *10*, 6720.
- [50] W. Chen, X. Li, Y. Li, Y. Li, *Energy Environ. Sci.* **2020**, *13*, 1971.
- [51] I. A. Howard, T. Abzieher, I. M. Hossain, H. Eggers, F. Schackmar, S. Ternes, B. S. Richards, U. Lemmer, U. W. Paetzold, *Adv. Mater.* **2019**, *31*, 1806702.
- [52] S. W. Dai, B. W. Hsu, C. Y. Chen, C. A. Lee, H. Y. Liu, H. F. Wang, Y. C. Huang, T. L. Wu, A. Manikandan, R. M. Ho, C. S. Tsao, C. H. Cheng, Y. L. Chueh, H. W. Lin, *Adv. Mater.* **2018**, *30*, 1705532.
- [53] X. Lao, Y. Bao, S. Xu, *Opt. Lett.* **2020**, *45*, 3881.
- [54] C. Luo, C. Yan, Wen Li, F. Chun, M. Xie, Z. Zhu, Y. Gao, B. Guo, W. Yang, *Adv. Funct. Mater.* **2020**, *30*, 2000026.
- [55] Y. Cai, H. Wang, Y. Li, L. Wang, Y. Lv, X. Yang, R. J. Xie, *Chem. Mater.* **2019**, *31*, 881.
- [56] Z. Li, K. Cao, J. Li, Y. Tang, X. Ding, B. Yu, *Opto-Electron. Adv.* **2021**, *4*, 02200019.
- [57] X. Li, Z. Wen, S. Ding, F. Fang, B. Xu, J. Sun, C. Liu, K. Wang, X. W. Sun, *Adv. Opt. Mater.* **2020**, *8*, 2000232.
- [58] Y. Yin, Z. Hu, M. U. Ali, M. Duan, L. Gao, M. Liu, W. Peng, J. Geng, S. Pan, Y. Wu, J. Hou, J. Fan, D. Li, X. Zhang, H. Meng, *Adv. Mater. Technol.* **2020**, *5*, 2000251.
- [59] F. Feng, K. Zhang, Y. Liu, Y. Lin, K. Xu, H. S. Kwok, Z. Liu, *IEEE Electron Device Lett.* **2021**, *43*, 60.
- [60] M. A. Boles, D. Ling, T. Hyeon, D. V. Talapin, *Nat. Mater.* **2016**, *15*, 141.
- [61] W. K. Bae, Y. S. Park, J. Lim, D. Lee, L. A. Padilha, H. McDaniel, I. Robel, C. Lee, J. M. Pietryga, V. I. Klimov, *Nat. Commun.* **2013**, *4*, 2661.
- [62] Y. S. Park, W. K. Bae, J. M. Pietryga, V. I. Klimov, *ACS Nano* **2014**, *8*, 7288.
- [63] Y. F. Shu, X. Lin, H. Y. Qin, Z. Hu, Y. Z. Jin, X. G. Peng, *Angew. Chem., Int. Ed.* **2020**, *59*, 22312.
- [64] Y. Shirasaki, G. J. Supran, M. G. Bawendi, V. Bulović, *Nat. Photonics* **2013**, *7*, 13.
- [65] H. Kim, S. R. Bae, T. H. Lee, H. Lee, H. Kang, S. Park, H. W. Jang, S. Y. Kim, *Adv. Funct. Mater.* **2021**, *31*, 2102770.
- [66] Q. Zeng, X. Zhang, Q. Bing, Y. Xiong, F. Yang, H. Liu, J. Y. Liu, H. Zhang, W. Zheng, A. L. Rogach, B. Yang, *ACS Energy Lett.* **2022**, *7*, 1963.
- [67] C. Sun, Y. Zhang, C. Ruan, C. Yin, X. Wang, Y. Wang, W. W. Yu, *Adv. Mater.* **2016**, *28*, 10088.
- [68] J. Li, Z. Li, J. Qiu, J. Li, *Adv. Opt. Mater.* **2022**, *10*, 2102201.
- [69] J. S. Li, Y. Tang, Z. T. Li, G. W. Liang, X. R. Ding, B. H. Yu, *IEEE Trans. Device Mater. Reliab.* **2018**, *19*, 120.
- [70] Z. T. Li, C. J. Song, Z. Y. Qiu, J. S. Li, K. Cao, X. R. Ding, Y. Tang, *IEEE Trans. Electron Devices* **2019**, *66*, 3020.
- [71] Z. T. Li, J. X. Li, J. S. Li, X. W. Du, C. J. Song, Y. Tang, *IEEE Trans. Electron Devices* **2019**, *66*, 4817.

- [72] Z. T. Li, Y. J. Chen, J. S. Li, S. M. Liang, Y. Tang, *Appl. Therm. Eng.* **2020**, *179*, 115666.
- [73] A. V. Malko, A. A. Mikhailovsky, M. A. Petruska, J. A. Hollingsworth, V. I. Klimov, *J. Phys. Chem. B* **2004**, *108*, 5250.
- [74] W. Lin, W. Zou, Z. J. Du, H. Q. Li, C. Zhang, *J. Nanopart. Res.* **2013**, *15*, 1629.
- [75] T. Han, Y. Yuan, X. Liang, Y. Zhang, C. Xiong, L. Dong, *J. Mater. Chem. C* **2017**, *5*, 4629.
- [76] F. Fang, M. J. Liu, W. Chen, H. C. Yang, Y. Z. Liu, X. Li, J. J. Hao, B. Xu, D. Wu, K. Cao, W. Lei, P. Muller-Buschbaum, X. W. Sun, R. Chen, K. Wang, *Adv. Opt. Mater.* **2020**, *8*, 1902118.
- [77] H. Q. Wang, H. Qian, Z. X. Luo, K. Y. Zhang, X. F. Shen, Y. Zhang, M. T. Zhang, F. Liebner, *Carbohydr. Polym.* **2019**, *224*, 115173.
- [78] H. Wang, Z. Shao, M. Bacher, F. Liebner, T. Rosenau, *Cellulose* **2013**, *20*, 3007.
- [79] Y. Altintas, S. Genc, M. Y. Talpur, E. Mutlugun, *Nanotechnology* **2016**, *27*, 295604.
- [80] D. H. Jiang, Y. H. Tsai, L. Veeramuthu, F. C. Liang, L. C. Chen, C. C. Lin, T. Satoh, S. H. Tung, C. C. Kuo, *APL Mater.* **2019**, *7*, 111105.
- [81] T. Otto, M. Muller, P. Mundra, V. Lesnyak, H. V. Demir, N. Gaponik, A. Eychmuller, *Nano Lett.* **2012**, *12*, 5348.
- [82] M. Adam, Z. Wang, A. Dubavik, G. M. Stachowski, C. Meerbach, Z. Soran-Erdem, C. Rengers, H. V. Demir, N. Gaponik, A. Eychmüller, *Adv. Funct. Mater.* **2015**, *25*, 2638.
- [83] W. Xu, Z. Cai, F. Li, J. Dong, Y. Wang, Y. Jiang, X. Chen, *Nano Res.* **2017**, *10*, 2692.
- [84] Y. Li, Y. Lv, Z. Guo, L. Dong, J. Zheng, C. Chai, N. Chen, Y. Lu, C. Chen, *ACS Appl. Mater. Interfaces* **2018**, *10*, 15888.
- [85] Y. Wang, J. He, H. Chen, J. Chen, R. Zhu, P. Ma, A. Towers, Y. Lin, A. J. Gesquiere, S.-T. Wu, Y. Dong, *Adv. Mater.* **2016**, *28*, 10710.
- [86] C. Kang, C. Lin, C. Lin, T. Li, S. Huang Chen, C. Tsai, C. Sher, T. Wu, P. Lee, X. Xu, M. Zhang, C. Ho, J. He, H. Kuo, *Adv. Sci.* **2019**, *6*, 1902230.
- [87] T. Y. Li, X. Xu, C. H. Lin, X. Guan, W. H. Hsu, M. L. Tsai, X. Fang, T. Wu, J. H. He, *Adv. Sci.* **2020**, *7*, 1902439.
- [88] H. Zhang, Z. Cui, Y. Wang, K. Zhang, X. L. Ji, C. L. Lv, B. Yang, M. Y. Gao, *Adv. Mater.* **2003**, *15*, 777.
- [89] H. Y. Kim, D. E. Yoon, J. Jang, G. M. Choi, D. C. Lee, B. S. Bae, *J. Soc. Inf. Disp.* **2017**, *25*, 108.
- [90] J. Jang, D. E. Yoon, S. M. Kang, Y. H. Kim, I. Lee, H. Lee, Y. H. Kim, D. C. Lee, B. S. Bae, *Nanoscale* **2019**, *11*, 14887.
- [91] Y. H. Kim, H. Lee, S. M. Kang, B. S. Bae, *ACS Appl. Mater. Interfaces* **2019**, *11*, 22801.
- [92] M. J. Smith, S. T. Malak, J. Jung, Y. J. Yoon, C. H. Lin, S. Kim, K. M. Lee, R. Ma, T. J. White, T. J. Bunning, Z. Lin, V. V. Tsukruk, *ACS Appl. Mater. Interfaces* **2017**, *9*, 17435.
- [93] J. S. Li, Y. Tang, Z. T. Li, L. S. Rao, X. R. Ding, B. H. Yu, *Photonics Res.* **2018**, *6*, 1107.
- [94] J. Li, Y. Tang, Z. Li, X. Ding, L. Rao, B. Yu, *Opt. Lett.* **2019**, *44*, 90.
- [95] H. Wang, Y. H. Xing, J. X. Li, J. Tan, Z. T. Li, C. H. Song, J. S. Li, *IEEE Electron Device Lett.* **2021**, *42*, 533.
- [96] C. Sun, X. Shen, Y. Zhang, Y. Wang, X. Chen, C. Ji, H. Shen, H. Shi, Y. Wang, W. W. Yu, *Nanotechnology* **2017**, *28*, 365601.
- [97] J. S. Li, Y. Tang, Z. T. Li, W. Q. Kang, X. R. Ding, B. H. Yu, *J. Electron. Packag.* **2019**, *141*, 041006.
- [98] Z. T. Li, C. J. Song, X. W. Du, J. Xuan, J. S. Li, Y. Tang, *IEEE Trans. Electron Devices* **2020**, *67*, 2418.
- [99] Z. T. Li, J. X. Li, Z. H. Deng, J. Y. Liang, J. S. Li, *IEEE Trans. Electron Devices* **2021**, *68*, 1738.
- [100] Y. Tang, Z. Li, Z. Li, J. Li, S. Yu, L. Rao, *IEEE Trans. Electron Devices* **2018**, *65*, 158.
- [101] Z. T. Li, J. X. Li, J. S. Li, Z. H. Deng, Y. H. Deng, Y. Tang, *IEEE J. Quantum Electron.* **2020**, *56*, 1.
- [102] J. S. Li, Y. Tang, Z. T. Li, Z. Li, X. R. Ding, L. S. Rao, *IEEE J. Sel. Top. Quantum Electron.* **2017**, *23*, 1.
- [103] D. Theobald, S. Yu, G. Gomard, U. Lemmer, *ACS Photonics* **2020**, *7*, 1452.
- [104] H. Lee, Y. H. Kim, Y. W. Lim, J. Jang, S. M. Kang, B. S. Bae, *Adv. Opt. Mater.* **2020**, *8*, 1902178.
- [105] H. C. Wang, S. Y. Lin, A. C. Tang, B. P. Singh, H. C. Tong, C. Y. Chen, Y. C. Lee, T. L. Tsai, R. S. Liu, *Angew. Chem., Int. Ed. Engl.* **2016**, *55*, 7924.
- [106] X. J. Zhang, H. C. Wang, A. C. Tang, S. Y. Lin, H. C. Tong, C. Y. Chen, Y. C. Lee, T. L. Tsai, R. S. Liu, *Chem. Mater.* **2016**, *28*, 8493.
- [107] J. Shen, Y. Wang, Y. Zhu, Y. Gong, C. Li, *Nanoscale* **2021**, *13*, 6586
- [108] Z. T. Li, C. J. Song, J. S. Li, G. W. Liang, L. S. Rao, S. D. Yu, X. R. Ding, Y. Tang, B. H. Yu, J. Z. Ou, U. Lemmer, G. Gomard, *Adv. Mater. Technol.* **2020**, *5*, 1900941.
- [109] J. Li, Y. Tang, Z. Li, X. Ding, B. Yu, L. Lin, *ACS Appl. Mater. Interfaces* **2019**, *11*, 18808.
- [110] Z. Li, J. Zheng, J. Li, W. Zhan, Y. Chen, *IEEE Photonics Technol. Lett.* **2021**, *33*, 727.
- [111] J. Li, Y. Tang, Z. Li, J. Li, X. Ding, B. Yu, S. Yu, J. Ou, H. Kuo, *ACS Nano* **2021**, *15*, 550.
- [112] Y. Xie, C. Geng, Y. Gao, J. G. Liu, Z. H. Zhang, Y. Zhang, S. Xu, W. Bi, *Materials* **2017**, *10*, 1242.
- [113] S. Yu, B. Fritz, S. Johnsen, D. Busko, B. S. Richards, M. Hippler, G. Wiegand, Y. Tang, Z. Li, U. Lemmer, H. Hölscher, G. Gomard, *Adv. Opt. Mater.* **2019**, *7*, 1900223.
- [114] B. Yu, Z. Huang, D. Fang, S. Yu, T. Fu, Y. Tang, Z. Li, *Adv. Mater. Interfaces* **2022**, *9*, 2101485.
- [115] G. Y. Kim, S. Kim, J. Choi, M. Kim, H. Lim, T. W. Nam, W. Choi, E. N. Cho, H. J. Han, C. Lee, J. C. Kim, H. Y. Jeong, S. Choi, M. S. Jang, D. Y. Jeon, Y. S. Jung, *Nano Lett.* **2019**, *19*, 6827.
- [116] J. H. Kang, B. Li, T. Zhao, M. A. Johar, C. C. Lin, Y. H. Fang, W. H. Kuo, K. L. Liang, S. Hu, S. W. Ryu, J. Han, *ACS Appl. Mater. Interfaces* **2020**, *12*, 30890.
- [117] H. Y. Liang, H. G. Zhao, Z. P. Li, C. Harnagea, D. L. Ma, *Nanoscale* **2016**, *8*, 4882.
- [118] G. Lu, Z. Yang, K. Zheng, S. Lin, J. Liu, B. Ye, J. Huang, Y. Zhang, Y. Ye, T. Guo, G. Chen, *Org. Electron.* **2020**, *77*, 105540.
- [119] M. Praveena, R. Dutta, J. K. Basu, *Plasmonics* **2017**, *12*, 1911.
- [120] S. Yu, B. Zhuang, J. Chen, Z. Li, L. Rao, B. Yu, Y. Tang, *Opt. Lett.* **2017**, *42*, 4962.
- [121] J. Li, Y. Tang, Z. Li, X. Ding, S. Yu, B. Yu, *Nanomaterials* **2018**, *8*, 508.
- [122] Z. T. Li, J. Y. Liang, J. S. Li, J. X. Li, Y. Tang, *J. Electron. Packag.* **2021**, *143*, 021002.
- [123] G. Liang, S. Yu, Y. Tang, Z. Lu, Y. Yuan, Z. Li, J. Li, *IEEE Trans. Electron Devices* **2020**, *67*, 4530.
- [124] B. Yu, Q. Zhao, Q. Li, J. Li, Z. Li, *IEEE Trans. Electron Devices* **2021**, *68*, 4522.
- [125] J. Lee, K. Min, Y. Park, K. S. Cho, H. Jeon, *Adv. Mater.* **2018**, *30*, 1703506.
- [126] J. Chen, D. Theobald, A. B. Shams, Q. Jin, A. Mertens, G. Gomard, U. Lemmer, *ACS Appl. Nano Mater.* **2021**, *5*, 87.
- [127] D. Venkatakrisnharao, C. Sahoo, R. Vattikunta, M. Annadhasan, S. R. G. Naraharisetty, R. Chandrasekar, *Adv. Opt. Mater.* **2017**, *5*, 1700695.
- [128] H. V. Han, H. Y. Lin, C. C. Lin, W. C. Chong, J. R. Li, K. J. Chen, P. Yu, T. M. Chen, H. M. Chen, K. M. Lau, H. C. Kuo, *Opt Express* **2015**, *23*, 32504.
- [129] H. Y. Lin, C. W. Sher, D. H. Hsieh, X. Y. Chen, H. M. P. Chen, T. M. Chen, K. M. Lau, C. H. Chen, C. C. Lin, H. C. Kuo, *Photonics Res.* **2017**, *5*, 411.
- [130] M. Duan, Z. Feng, Y. Wu, Y. Yin, Z. Hu, W. Peng, D. Li, S. J. Chen, C. Y. Lee, A. Lien, *Adv. Mater. Technol.* **2019**, *4*, 1900779.

- [131] L. Shi, L. Meng, F. Jiang, Y. Ge, F. Li, X. G. Wu, H. Zhong, *Adv. Funct. Mater.* **2019**, *29*, 1903648.
- [132] S. J. Ho, H. C. Hsu, C. W. Yeh, H. S. Chen, *ACS Appl. Mater. Interfaces* **2020**, *12*, 33346.
- [133] B. H. Kim, M. S. Onses, J. B. Lim, S. Nam, N. Oh, H. Kim, K. J. Yu, J. W. Lee, J. H. Kim, S. K. Kang, C. H. Lee, J. Lee, J. H. Shin, N. H. Kim, C. Leal, M. Shim, J. A. Rogers, *Nano Lett.* **2015**, *15*, 969
- [134] S. W. Wang, K. Hong, Y. Tsai, C. Teng, A. Tzou, Y. Chu, P. Lee, P. Ku, C. Lin, H. Kuo, *Sci. Rep.* **2017**, *7*, 42962.
- [135] S. W. H. Chen, C. C. Shen, T. Wu, Z. Y. Liao, L. F. Chen, J. R. Zhou, C.-F. Lee, C.-H. Lin, C.-C. Lin, C.-W. Sher, P.-T. Lee, A.-J. Tzou, Z. Chen, H.-C. Kuo, *Photonics Res.* **2019**, *7*, 416.
- [136] H. Li, Y. Duan, Z. Shao, G. Zhang, H. Li, Y. Huang, Z. Yin, *Adv. Mater. Technol.* **2020**, *5*, 2000401.
- [137] C. Zhao, H. Li, Y. Wang, K. Li, J. Hou, Y. Ma, M. Li, Y. Song, *Adv. Opt. Mater.* **2019**, *7*, 1900127.
- [138] H. M. Kim, M. Ryu, J. H. J. Cha, H. S. Kim, T. Jeong, J. Jang, *J. Soc. Inf. Disp.* **2019**, *27*, 347.
- [139] X. Li, D. Kundaliya, Z. J. Tan, M. Anc, N. X. Fang, *Opt Express* **2019**, *27*, 30864.
- [140] Y. H. Kim, S. Koh, H. Lee, S. M. Kang, D. C. Lee, B. S. Bae, *ACS Appl. Mater. Interfaces* **2019**, *12*, 3961.
- [141] J. S. Park, J. Kyhm, H. H. Kim, S. Jeong, J. Kang, S. E. Lee, K. T. Lee, K. Park, N. Barange, J. Han, J. D. Song, W. K. Choi, I. K. Han, *Nano Lett.* **2016**, *16*, 6946.
- [142] H. L. Kang, J. Kang, J. K. Won, S. M. Jung, J. Kim, C. H. Park, B. K. Ju, M. G. Kim, S. K. Park, *Adv. Opt. Mater.* **2018**, *6*, 1701335.
- [143] W. Xie, R. Gomes, T. Aubert, S. Bisschop, Y. Zhu, Z. Hens, E. Brainis, D. V. Thourhout, *Nano Lett.* **2015**, *15*, 7481.
- [144] F. Palazon, Q. A. Akkerman, M. Prato, L. Manna, *ACS Nano* **2016**, *10*, 1224.
- [145] B. B. Xu, Y. L. Zhang, R. Zhang, L. Wang, X. Z. Xiao, H. Xia, Q. D. Chen, H. B. Sun, *J. Mater. Chem.* **2013**, *1*, 4699.
- [146] W. Zhan, L. Meng, C. Shao, X.-g. Wu, K. Shi, H. Zhong, *ACS Photonics* **2021**, *8*, 765.
- [147] J. Chen, Y. Wu, X. Li, F. Cao, Y. Gu, K. Liu, X. Liu, Y. Dong, J. Ji, H. Zeng, *Adv. Mater. Technol.* **2017**, *2*, 1700132.
- [148] Z. T. Li, J. Y. Qi, J. S. Li, Q. L. Zhao, R. X. Qian, Z. H. Deng, *J. Mater. Process. Technol.* **2023**, *313*, 117873.
- [149] T. H. Kim, K. S. Cho, E. K. Lee, S. J. Lee, J. Chae, J. W. Kim, D. H. Kim, J. Y. Kwon, G. Amaratunga, S. Y. Lee, B. L. Choi, Y. Kuk, J. M. Kim, K. Kim, *Nat Photonics* **2011**, *5*, 176.
- [150] M. K. Choi, J. Yang, K. Kang, D. C. Kim, C. Choi, C. Park, S. J. Kim, S. I. Chae, T. Kim, J. Kim, T. Hyeon, D. Kim, *Nat. Commun.* **2015**, *6*, 7149.
- [151] J. Bae, Y. Shin, H. Yoo, Y. Choi, J. Lim, D. Jeon, I. Kim, M. Han, S. Lee, *Nat. Commun.* **2022**, *13*, 1862.
- [152] E.-L. Hsiang, Y. Li, Z. He, T. Zhan, C. Zhang, Y.-F. Lan, Y. Dong, S.-T. Wu, *J. Soc. Inf. Disp.* **2021**, *29*, 288.
- [153] PlayNitride, Micro-LED panel, <https://www.playnitride.com/en/news/may-2022-playnitride-showcases-new-microled-commercialization-solutions-at-sid-display-week-2022-focusing-on-automotives-consumer-electronics-products-and-ar-applications> (accessed: May **2022**).
- [154] JBD, Micro-LED projector, <https://www.jb-display.com/company/125.html> (accessed: May **2023**).



**Junchi Chen** is currently a Ph.D. student at Light Technology Institute (LTI), Karlsruhe Institute of Technology (KIT). He received his Bachelor's degree in 2017 and his Master's degree in 2019 from South China University of Technology (SCUT). His research focuses on the light management and the color conversion of quantum dot materials.



**Uli Lemmer** received his Diploma degree from RWTH Aachen University in 1990 and a Ph.D. from the University of Marburg in 1995. He then held a postdoctoral position with the University of California at Santa Barbara. Afterward, he was heading the Organic Optoelectronics group at the University of Munich from 1996 to 2002. In 2002 he was appointed as Full Professor of Electrical Engineering and Information Technology and Director of the Light Technology Institute, Karlsruhe Institute of Technology (KIT). His research interests are in the field of optoelectronics and the technology and the applications of printable organic and inorganic materials.